Fluoresenssin elinaika ja anisotropia [Työ D1, tutkiva valokemia, 2 op]

Jyväskylän yliopisto
Kemian laitos
KEMS4800 – Optisen spektroskopian työt
Työohje, 2017–2018

Tiivistelmä

Työssä opitaan määrittämään väriaineelle fluoresenssin elinaika ja rotaatiokorrelaatioaika. Mittaukset tehdään Nanotiedekeskuksen laboratoriotiloissa.

1 Johdanto

Työssä mitataan yksittäisfotonilaskentalaitteistolla (single photon counting, SPC) eosiinimolekyylille fluoresenssin elinaika, sekä määritetään anisotropiamittauksen avulla molekyylin rotaatiokorrelaatioaika eli aika, jossa molekyyli pyörähtää yhden radiaanin etanoliliuoksessa. Rotaatiokorrelaatioajan avulla voidaan arvioida mm. molekyylin kokoa. Mittaukset tehdään sekä huoneenlämpötilassa että jäähdytetystä näytteestä, ja tutkitaan kuinka lämpötilan muutos vaikuttaa fluoresenssiin ja molekyylin liikkeeseen.

2 Teoria

Yksittäisfotonilaskennan yleiset periaatteet (Liitteet 1 ja 2):

- Kaaviokuva laitteistosta (tarvittavat optiset komponentit).
- Miksi count rate pitää olla $<1/100$ virityspulssien taajudesta?
- Mitä tarkoittaa aikaresoluutio ja mitkä tekijät sitä rajoittavat?

Anisotropian käsite (Liitteet 2 ja 3):

- Mitä tarkoittaa magic angle?
- Mitä tarkoittaa stick/slip-model rotaatiokorrelaatiossa?
- Mitä oletuksia molekyylistä Stokesin, Einsteinin ja Debyen yhtälössä tehdään? Ovatko ne järkeviä tässä tapauksessa?

3 Työn suoritus

1. Valmistetaan tutkittava näyte eosiini-väriaineesta käyttäen liuottimena etanolia (spektroskopinen laatu).

2. Mitataan näytteen absorptio- ja fluoresenssispektrit. Säädetään näytteen konsentraatio sellaiseksi, että sen absorbanssi on n. 0,1 viritysaallonpituudella 485 nm.

3. Tutustutaan yksittäisfotonilaskentalaitteiston osiin.

4. Määritetään laitteiston aikaresoluutio eli kuinka lyhyitä aikaskaaloja laitteella voidaan luotettavasti havaita. Tämä tehdään mittaamalla virittävän valon sironnasta syntyvää signaalia.

5. Mitataan eosiinille fluoresenssin elinaika huoneenlämpötilassa.

6. Tehdään anisotropiamittaus eli mitataan erikseen fluoresenssisignaalit, joiden polarisaatio on yhdensuuntainen ja kohtisuora viritysvalon polarisaatioon nähden.

7. Jäähdytetään näyte nestetyppikryostaatin avulla ja toistetaan mittaukset jäähdytetystä näytteestä.

4 Tulosten tarkastelu

- Esitetään absorptio- ja fluoresenssispektrit. Näytteen konsentraation voi laskea eosiinin molaarisen absorptiokertoimen avulla.

- Arvioidaan tehtyjen mittausten aikaresoluutiosta.

- Määritetään fluoresenssin elinaika eosiinille. Tuotetaan magic angle -signaali ja sovitetaan Originilla “exponential decay”. Tarkastellaan, onko eroa eri lämpötiloissa.

- Määritetään fluoresenssin anisotropian palautumisaika eli rotaatiokorrelaatioaika molemmissa lämpötiloissa. Sovitetaan tässäkin eksponenttifunktio.

- Määritetään molekyylin tilavuus molemmissa lämpötiloissa käyttämällä Stokesin, Einsteinin ja Debyen yhtälöä. Viskositeetin eri lämpötiloissa voi laskea yhtälöstä[1]

$$\ln \eta = -7{,}1056 + 1675\, T^{-1} + 0{,}0103679\, T - 1{,}71008 \times 10^{-5}\, T^2\,,$$

  missä η on viskositeetti yksikössä mPa s ja T on lämpötila kelvineissä.

- Kommentoidaan ovatko tulokset järkeviä. Havaintoja ja pohdintoja työstä ja tuloksista.

Kirjallisuusarvoja:
Fluoresenssin elinaika $\tau = 3{,}620 \pm 0{,}225$ ns.[2]
Rotaatiokorrelaatioaika $\tau_{\mathrm{rot}} = 420 \pm 30$ ps.[3]

Liitteet

Liite 1: TC-SPC Technical Note, PicoQuant GmbH, 11 sivua.

Liite 2: Otteita kirjasta Lakowicz, Principles of Fluorescence Spectroscopy, 8 sivua.

Liite 3: Tutkimusartikkeli (Biochem. Mol. Biol. Educ. 2003, 31, 319–322), 4 sivua.

Viitteet

1. Perry, R. H. ja Green, D. W., *Perry's Chemical Engineers' Handbook*, 7. painos, McGraw-Hill, New York, 1997.

2. Fleming, G. R.; Knight, A. W. E.; Morris, J. M.; Morrison, R. J. S. ja Robinson, G. W., Picosecond fluorescence studies of xanthene dyes, *J. Am. Chem. Soc.*, **1977**, *99*, 4306–4311.

3. von Jena, A. ja Lessing, H. E., Rotational-diffusion anomalies in dye solutions from transient-dichroism experiments, *Chem. Phys.*, **1979**, *40*, 245–256.

Technical Note

Time-Correlated Single Photon Counting

Michael Wahl, PicoQuant GmbH

The Principle of Time-Correlated Single Photon Counting

Time-resolved fluorescence spectroscopy is a powerful analysis tool in fundamental physics as well as in the life sciences. Implementing it in the time domain requires recording the time dependent intensity profile of the emitted light upon excitation by a short flash of light, typically a laser pulse. While in principle, one could attempt to record the time decay profile of the signal from a single excitation-emission cycle, there are practical problems preventing such a simple solution in most cases. First of all, the decay to be recorded is very fast. Typical fluorescence from important organic fluorophores lasts only some hundred picoseconds to some tens of nanoseconds. In order to recover not only fluorescence lifetimes but also the decay shape, one must be able to resolve the recorded signal at least to such an extent, that the decay is represented by some tens of samples. For a decay of, e.g., 500 ps this means the transient recorder required would have to sample at e.g. 50 ps time steps.

This is hard to achieve with ordinary electronic transient recorders. Moreover, the light available may be simply too weak to sample an analog time decay. Indeed the signal may consist of just a few photons per excitation /emission cycle. Then the discrete nature of the signal itself prohibits analog sampling. Even if one has some reserve to increase the excitation power to obtain more fluorescence light, there will be limits, e.g. due to collection optic losses, spectral limits of detector sensitivity or photo-bleaching at higher excitation power. The solution for both problems is Time-Correlated Single Photon Counting (TCSPC). With periodic excitation (e.g. from a laser) it is possible to extend the data collection over multiple cycles and one can reconstruct the single cycle decay profile from single photon events collected over many cycles.

The method is based on the repetitive precisely timed registration of single photons of e.g. a fluorescence signal [1,2]. The reference for the timing is the corresponding excitation pulse. As a single photon sensitive detector a Photomultiplier Tube (PMT), Micro Channel Plate (MCP) or a Single Photon Avalanche Diode (SPAD) can be used. Provided that the probability of registering more than one photon per cycle is low, the histogram of photon arrivals per time bin represents the time decay one would have obtained from a “single shot” time-resolved analog recording. The precondition of single photon probability can (and must) be met by simply attenuating the light level at the sample if necessary.

The following diagrams illustrate how the histogram is formed over multiple cycles. In the example, fluorescence is excited by laser pulses. The time difference between excitation and emission is measured by electronics that act like a stopwatch. If the single photon probability condition is met, there will actually be no photons at all in many cycles. In the example this situation is shown after the second laser pulse. It should be noted that the occurrence of a photon or an empty cycle is entirely random and can only be described in terms of probabilities. Indeed, the same holds true for the individual stopwatch readings.

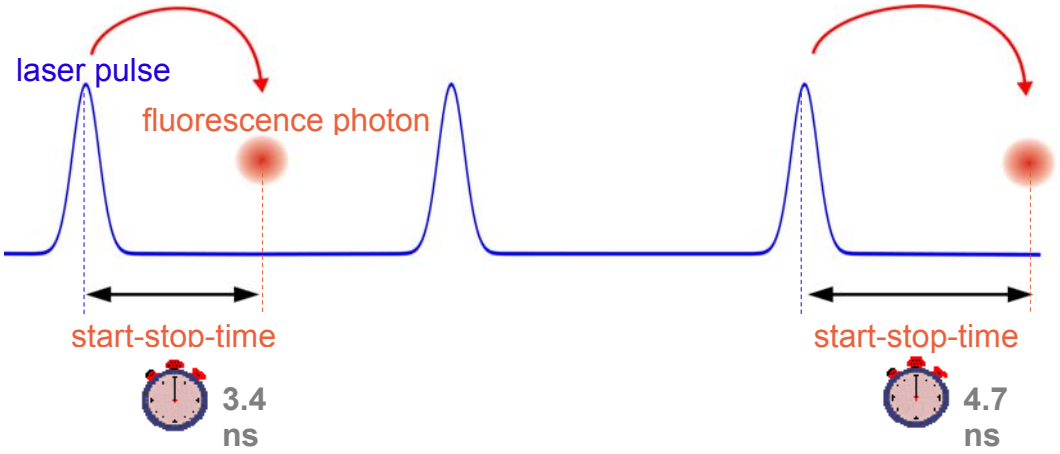

Fig. 1

The histogram is collected in a block of memory, where one memory cell holds the photon counts for one corresponding time bin. These time bins are often referred to as time channels. The typical result is a histogram with an exponential drop of counts towards later times.

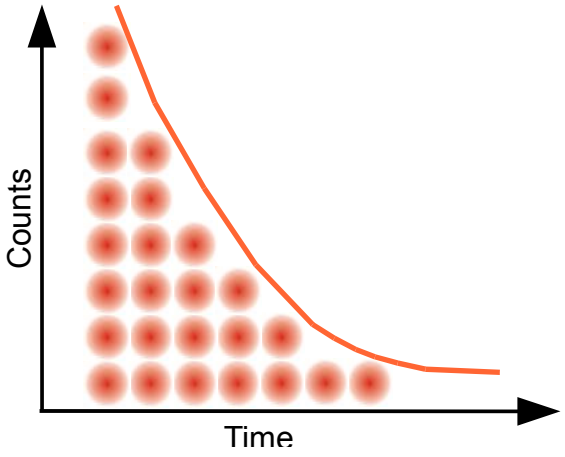

Fig. 2: Fluorescence lifetime histogram: exponential decay

In practice the registration of one photon involves the following steps: first the time difference between the photon event and the corresponding excitation pulse must be measured. For this purpose both events are converted to electrical signals. For the fluorescence photon this is done via the single photon detector mentioned before. For the excitation pulse it may be done via another detector if there is no electrical synchronisation signal (sync) supplied by the laser. Obviously, all conversion to electrical pulses must preserve the precise timing of the signals as accurately as possible.

The actual time difference measurement is done by means of fast electronics which provide a digital timing result. This digital timing result is then used to address the histogram memory so that each possible timing value corresponds to one memory cell or histogram bin. Finally the addressed histogram cell is incremented. All steps are carried out by fast electronics so that the processing time required for each photon event is as short as possible. When sufficient counts have been collected the histogram memory can be read out. The histogram data can then be used for display and e.g. fluorescence lifetime calculation. In the following sections we will expand on the various steps involved in the method and associated issues of importance.

Count rates and single photon statistics

It was mentioned that it is necessary to maintain a low probability of registering more than one photon per cycle. This is to guarantee that the histogram of photon arrivals represents the time decay one would have obtained from a single shot time-resolved analog recording. The reason for this is briefly the following: Detector and electronics have a "dead" time for at least some nanoseconds after a photon event. Because of these dead times TCSPC systems are usually designed to register only one photon per excitation cycle. If now the number of photons occurring in one excitation cycle were typically >1, the system would very often register the first photon but miss the following ones. This would lead to an over-representation of early photons in the histogram, an effect called 'pile-up'. It is therefore crucial to keep the probability of cycles with more than one photon low.

To quantify this demand one has to set acceptable error limits for the lifetime measurement and apply some statistics. For practical purposes one may use the following rule of thumb: In order to maintain single photon statistics, on average only one in 20..100 excitation pulses should generate a count at the detector. In other words: the average count rate at the detector should be at most 1..5% of the excitation rate. E.g. with the diode laser PDL 800-B, pulsed at 80 MHz repetition rate, the average detector count rate should not exceed 4 MHz. This leads to another issue: the count rate the system (of both detector and electronics) can handle. Indeed 4 MHz are stretching the limits of many detectors and certainly are way beyond the capabilities of most conventional NIM based TCSPC systems. On the other hand, one wants high count rates, in order to acquire fluorescence decay histograms quickly. This may be of particular importance where dynamic lifetime changes or fast molecule transitions are to be studied or where large numbers of lifetime samples must be collected (e.g. in 2D scanning configurations). PMTs (dependent on the design) can handle count rates of up to 1..10 Millions of counts per second (cps), standard (passively quenched) SPADs saturate at a few hundred kcps. Oldfashioned NIM based TCSPC electronics can handle a maximum of 50,000 to 500,000 cps. With modern integrated TCSPC designs count rates over 10 Mcps can be achieved. It is also worth noting that the actual count arrival times of course are random so that there can be bursts of high count rate and periods of low count rates. Bursts of photons may still exceed the average rate. This should be kept in mind when an experiment is planned. Even if an instrument can accommodate the average rate, it may drop photons in bursts. This is why the length of the dead-time is of interest too. This quantity describes the time the system cannot register photons while it is processing a previous photon event. The term is applicable to both detectors and electronics. Dead-time or insufficient throughput of the electronics are usually not of detrimental effect on the decay histogram or, more precisely, the lifetime to be extracted from the latter. However, the photon losses prolong the acquisition time or deteriorate the SNR if the acquisition time remains fixed. In applications where the photon burst density must be evaluated (e.g. for molecule transition detection or imaging) long dead-times can be a problem.

Timing resolution

The characteristic of a complete TCSPC system that summarizes its overall timing precision is its Instrument Response Function (IRF). The basic idea is that if the system is ideal, i.e. has an infinitely sharp excitation pulse and infinitely accurate detectors and electronics, it should have an infinitely narrow IRF. Any deviation from this ideal results in a broadening of the IRF. Before looking into how the individual error contributions add up, the most critical sources shall be introduced here.

The weakest component in terms of timing resolution in TCSPC measurements will usually be the detector. However, as opposed to analog transient recording, the time resolution of TCSPC is not limited by the pulse response of the detector. Only the timing accuracy of registering a photon determines the TCSPC resolution. The timing accuracy is limited by the timing uncertainty the detector introduces in the conversion from a photon to an electrical pulse. This timing error (or uncertainty) can be as much as 10 times smaller than the detectors pulse response. The timing uncertainties are usually quantified by specifying the r.m.s. error or the Full Width Half Maximum (FWHM) of the timing error distribution. Note that these two notations are related but not identical. In the case of a Gaussian error distribution the FWHM value is twice as large as the corresponding r.m.s. value. Good but also expensive detectors, notably MCPs, can achieve timing uncertainties as small as 25 ps FWHM. Cheaper PMTs or SPADs may introduce uncertainties of 200 to 400 ps FWHM. More recent SPADs can show timing uncertainties as small as 30 ps FWHM.

The second most critical source of IRF broadening usually is the excitation source. While most laser sources can provide sufficiently short pulses, it is also necessary to obtain an electrical timing reference signal (sync) to compare the fluorescence photon signal with. Where this signal is derived from depends on the excitation source. With gain switched diode lasers (e.g. PDL 800-B) a low jitter electrical sync signal is readily available. The signal type used here is commonly a narrow negative pulse of -800 mV into 50 Ohms (NIM standard). The very sharp falling edge is synchronous with the laser pulse (<3 ps r.m.s. jitter for the PDL 800-B). With other lasers (e.g. many Ti:Sa lasers) a second detector must be used to derive a sync signal from the optical pulse train. This is commonly done with a fast photo diode (APD or PIN diode, e.g. the TDA 200). The light for this reference detector must be coupled out from the excitation laser beam e.g. by means of some semi-transparent mirror. The reference detector must be chosen and set up carefully as it also contributes to the overall timing error.

Another source of timing error is the timing jitter of the electronic components used for TCSPC. This is caused by the finite rise/fall-time of the electric signals used for the time measurement. At the trigger point of e.g. compactors, logic gates etc. the amplitude noise (thermal noise, interference etc.) always present on these signals is transformed to a corresponding timing error (phase noise). However the contribution of the electronics to the total timing error usually is relatively small. Modern TCSPC electronics cause an r.m.s. jitter of <10 ps. Nevertheless it is always a good idea to keep the RF noise low. This is why signal leads should be properly shielded coax cables and strong sources of RF interference should be kept away from the TCSPC detector and electronics.

The contribution of the time spread introduced by the individual components of a TCSPC system to the total IRF width strongly depends on their relative magnitude. Strictly, the total IRF is the convolution of all component IRFs. An estimate of the overall IRF width can be obtained from the geometric sum of the individual components e.g. as r.m.s. error or FWHM (Full Width Half Maximum) values according to statistical error propagation laws:

$$e_{\mathrm{IRF\,system}} \approx \sqrt{\sum e^2_{\mathrm{component}}} \qquad (1)$$

Obviously, due to the squares in the sum, the total will be more than proportionally dominated by the largest component. It is therefore of little value to improve a component that is already relatively good. If e.g. the detector has an IRF width of 200 ps, shortening of the laser pulse from 50 ps to 40 ps is practically of no effect.

Apart from predicting the approximate IRF width according to Eqn. 1 one can of course measure it. The typical approach is to place a scattering medium in the sample compartment so that there is no fluorescence but only some scattered excitation light reaching the detector. The IRF measurement is not only a means of optimizing and testing the instrument. It also serves as an input to data analysis with „deconvolution“ and is therefore a frequent measurement task. It was mentioned earlier that the total IRF is the convolution of all component IRFs. Similarly, the measured fluorescence decay is the convolution of the „true“ physical process of exponential decay with the IRF. With this theoretical model it is possible to extract the parameters of the „true“ decay process [3]. This is often referred to as „deconvolution“ although it should be noted that the term is not mathematically precise in this context. The procedure that most data anaysis programs actually perform is an iterative reconvolution.

Having established the role of the IRF and possibly having determined it for a given instrument leads to the question what the actual lifetime measurement resolution of the instrument will be. Unfortunately it is difficult to specify a general lower limit on the fluorescence lifetime that can be measured by a given TCSPC instrument. Apart from the instrument response function and noise, factors such as quantum yield, fluorophore concentration, and decay kinetics will affect the measurement. However, as a rule of thumb one can assume that under favourable conditions, most importatntly sufficient counts in the histogram, lifetimes down to 1/10 of the IRF width (FWHM) can still be recovered via iterative reconvolution.

A final time-resolution related issue worth noting here is the bin width of the TCSPC histogram. As outlined above, the analog electronic processing of the timing signals (detector, amplifiers, etc.) creates a continuous (e.g. Gaussian) distribution around the true value. In order to form a histogram, at some point the timing results must be quantised into discrete time bins. This quantisation introduces another random error that can be detrimental if chosen too coarse. The time quantisation step width (i.e. the bin width) must therefore be small compared to the width of the analog error distribution. As a minimum from the information theoretical point of view one would assume the Nyquist frequency. I.e. an analog signal should be sampled at least at twice the highest frequency contained in it. The high frequency content depends on the shape of the distribution. In a basic approximation this can reasonably be assumed to be Gaussian and therefore having very little high frequency content. For practical purposes there is usually no point in collecting the histogram at time resolutions much higher than 1/10 of the width of the analog error distribution. Nevertheless, a good histogram resolution is helpful in data analysis with iterative reconvolution.

Photon counting detectors

Photomultiplier Tube (PMT)

A PMT consists of a light-sensitive photocathode that generates electrons when exposed to light. These electrons are directed onto a charged electrode called a dynode. The collision of the electrons with the dynode produces additional electrons. Since each electron that strikes the dynode causes several electrons to be emitted, there is a multiplication effect. After further amplification by multiple dynodes, the electrons are collected at the anode of the PMT and output as a current. The current is directly proportional to the intensity of light striking the photocathode. Because of the multiplicative effect of the dynode chain, the PMT is a photoelectron amplifier of high sensitivity and remarkably low noise. PMTs have a wide dynamic range, i.e. they can also measure relatively high levels of light. They furthermore are very fast, so rapid successive events can be reliably monitored. PMTs are also quite robust. The high voltage driving the tube may be varied to change the sensitivity of the PMT.

When the light levels are as low as in TCSPC the PMT „sees“ only individual photons. One photon on the photocathode produce a short output pulse containing millions of photoelectrons. PMTs can therefore be used as single photon detectors. In photon counting mode, individual photons that strike the photocathode of the PMT are registered. Each photon event gives rise to an electrical pulse at the output. The number of pulses, or counts per second, is proportional to the light impinging upon the PMT. As the number of photon events increase at higher light levels, it will become difficult to differentiate between individual pulses and the photon counting detector will become non-linear. Dependent on the PMT design this usually occurs at 1-10 millions of counts per second.

The timing uncertainty between photon arrival and electrical output is small enough to permit time-resolved photon counting at a sub-nanosecond scale. In single photon counting mode the tube is typically operated at a constant high voltage where the PMT is most sensitive.

PMTs usually operate between the blue and red regions of the visible spectrum, with greater quantum efficiency in the blue-green region, depending upon photo-cathode materials. Typical peak quantum efficiencies are about 25%. For spectroscopy experiments in the ultraviolet and visible region of the spectrum, a photomultiplier tube is very well suited. In the near infrared the sensitivity drops off rapidly. Optimized cathode materials can be used to push this limit, which may on the other hand lead to increased noise. The latter can to some extent be reduced by cooling.

Because of noise from various sources in the tube, the output of the PMT may contain pulses that are not related to the light input. These are referred to as dark counts. The detection system can to some extent reject these spurious pulses by means of electronic discriminator circuitry. This discrimination is based on the probability that some of the noise generated pulses (those from the dynodes) exhibit lower signal levels than pulses from a photon event.

Microchannel Plate PMT (MCP)

A microchannel plate PMT is also a sensitive photon detector. It consists of an array of glass capillaries (10-25 µm inner diameter) that are coated on the inside with a electron-emissive material. The capillaries are biased at a high voltage applied across their length. Like in the PMT, an electron that strikes the inside wall of one of the capillaries creates an avalanche of secondary electrons. This cascading effect creates a gain of 103 to 106 and produces a current pulse

at the output. Due to the confined paths the timing jitter of MCPs is sufficiently small to perform time-resolved photon counting on a sub-nanosecond-scale, usually outperforming PMTs. Good but also expensive MCPs can achieve timing uncertainties as low as 25 ps. Microchannel plates are also used as an intensifier for low-intensity light detection with array detectors.

Avalanche Photo Diode (APD)

APDs are the semiconductor equivalent of PMTs. Generally, APDs may be used for ultra-low light detection (optical powers <1 pW), and can be used in either "linear" mode (bias voltage slightly less than the breakdown voltage) at gains up to about 500, or as photon-counters in the so-called "Geiger" mode (biased slightly above the breakdown voltage). In the case of the latter, the term gain is meaningless. A single photon may trigger an avalanche of about 108 carriers but one is not interested in the output current or voltage because it carries no information other than „there was a photon“. Instead, in this mode the device can be used as a detector for photon counting with very accurate timing of the photon arrival. In this context APDs are referred to as Single Photon Avalanche Diodes (SPAD). Widespread commercial products attain timing accuracies on the order of 400 ps FWHM. Single-photon detection probabilities of up to approximately 50% are possible. Maximum quantum efficiencies reported are about 80%. More recent SPAD designs focus on timing resolution and can achieve timing accuracies down to 30 ps but are less sensitive at the red end of the spectrum. The dark count rate (noise) of SPADs strongly depends on the active area. In SPADs it is much smaller than in PMTs, which can make optical interfacing difficult.

Other and novel detectors

The field of photon detectors is still evolving. Recent developments that are beginning to emerge as usable products include so called silicon PMTs, Hybrid PMTs, superconducting nanowire detectors and APDs with sufficient gain for single photon detection in analog mode. Each of these detectors have their specific benefits and shortcomings. Only a very brief overview can be given here. Silicon PMTs are essentially arrays of SPADs, all coupled to a common output. This has the benefit of creating a large area detector that can even resolve photon numbers. The drawback is increased dark count rate and relatively poor timing accuracy. Hybrid PMTs make use of a combination of a PMT front end followed by an APD structure. The benefits are good timing and virtually zero afterpulsing while the need for very high voltage is a disadvantage. Superconducting nanowires (typically made from NbN) can be used to create photon detectors with excellent timing performance and high sensitivity reaching into the infrared. The shortcomings for practical purposes are the extreme cooling requirements and the low fill factor of the wire structures, making it difficult to achieve good collection efficiencies. Another class of potentially interesting detectors are recently emerging APDs with very high gain. In combination with a matched electronic amplifier they have been shown to detect single photons. As opposed to Geiger mode, this avoids afterpulsing and allows very fast counting rates. The disadvantage is a high dark count rate, currently way too high for any practical TCSPC application.

Basic principles behind the TCSPC electronics

Conventional TCSPC systems consist of the following building blocks (Fig. 3):

The CFD is used to extract precise timing information from the electrical detector pulses that may vary in amplitude. This way the overall system IRF may be tuned to become narrower. The same could not be achieved with a simple threshold detector (comparator). Particularly with PMTs, constant fraction discrimination is very important as their pulse amplitudes vary significantly. The figures 4 and 5 show a comparison between level trigger and CFD operation.

The most common way of implementing a CFD is the comparison of the original detector signal with an amplified and delayed version of itself. The signal derived from this comparison changes its polarity exactly when a constant fraction of the detector pulse height is reached. The zero crossing point of this signal is therefore suitable to derive a timing signal independent from the amplitude of the input pulse. This is done by a subsequent comparison of this signal with a settable zero level, the so called zero cross trigger. Making this level settable allows to adapt to the noise

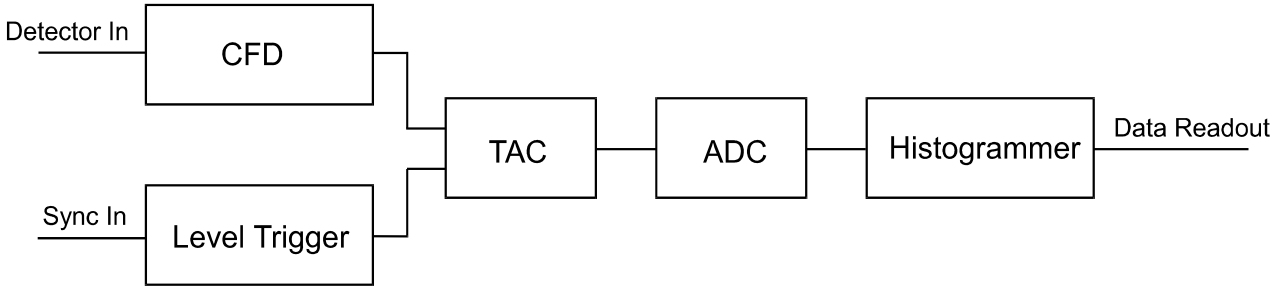

Fig. 3

levels in the given signal, since in principle an infinitely small signal could trigger the zero cross comparator. Typical CFDs furthermore permit the setting of a so called discriminator level, determining the lower limit the detector pulse amplitude must pass. Random background noise pulses can thereby be suppressed. Particularly pulses originating from random electrons generated at the dynodes of the PMT can be suppressed as they had less time to amplify, so that their output pulses are small.

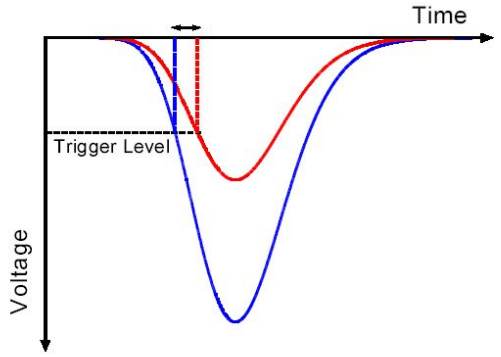

Fig. 4: Constant level trigger

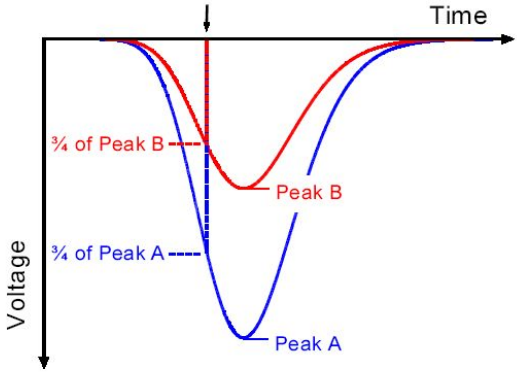

Fig. 5: Constant fraction trigger

Similar as for the detector signal, the sync signal must be made available to the timing circuitry. Since the sync pulses are usually of well-defined amplitude and shape, a simple settable comparator (level trigger) is sufficient to adapt to different sync sources.

In the classical design the signals from the CFD and SYNC trigger are fed to a Time to Amplitude Converter (TAC). This circuit is essentially a highly linear ramp generator that is started by one signal and stopped by the other. The result is a voltage proportional to the time difference between the two signals.

The voltage obtained from the TAC is then fed to an Analog to Digital Converter (ADC) which provides the digital timing value used to address the histogrammer. The ADC must be very fast in order to keep the dead time of the system short. Furthermore it must guarantee a very good linearity, over the full range as well as differentially. These are criteria difficult to meet simultaneously, particularly with ADCs of high resolution (e.g. 12 bits) as is desirable for TCSPC over many histogram channels. Furthermore, the TAC range is very limited.

The histogrammer has to increment each histogram memory cell whose digital address in the histogram memory it receives from the ADC. This is commonly done by fast digital logic e.g. in the form of Field Programmable Gate Arrays (FPGA) or a microprocessor. Since the histogram memory at some point also must be available for data readout, the histogrammer must stop processing incoming data. This prevents continuous data collection. Sophisticated TCSPC systems solve this problem by switching between two or more memory blocks, so that one is always available for incoming data.

While this section so far outlined the typical structure of conventional TCSPC systems, it is worth noting that the tasks performed by TAC and ADC can be carried out by a single fully digital circuit, a so called Time to Digital Converter (TDC). These circuits can measure time differences based on the delay times of signals in semiconductor logic gates or the conductor strips between them. The relative delay times in different gate chains can be used to determine time differences well below the actual gate delay. Other TDC designs use interpolation techniques between the pulses of a coarser clock. This permits exceptionally small, compact and affordable TCSPC solutions, as the circuits can be implemented as Application Specific Integrated Circuits (ASICS) at low cost and high reliability. All PicoQuant TCSPC systems make use of such a design. The historical starting point of the whole family of TDC based TCSPC systems was the TimeHarp 100 permitting a digital resolution of <40 ps (<150 ps analog FWHM). This resolution was well matched to the excitation pulse widths possible with diode lasers and the resolution permitted by affordable compact PMTs (e.g. IRF 200 ps). Later we introduced the TimeHarp 200 with PCI interface and slightly improved resolution. Figure 6 shows a basic block diagram of the TimeHarp 100/200. The TAC and ADC have been replaced by a TDC.

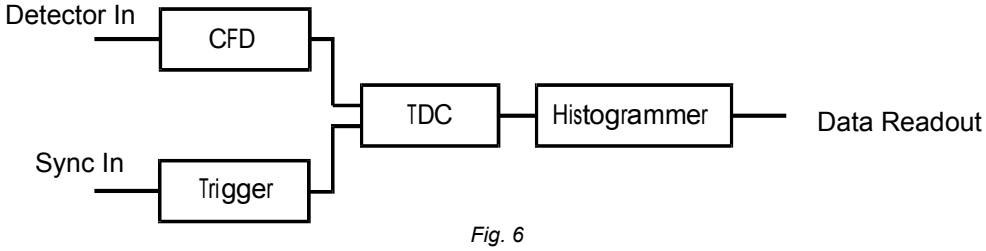

Fig. 6

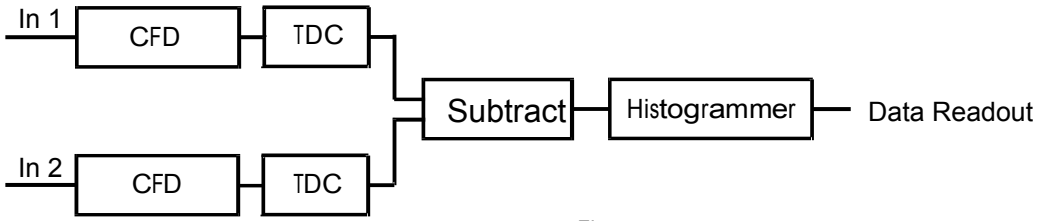

Fig. 7

The next significant steps were the PicoHarp 300 with 4 ps digital resolution and host interfacing via USB and finally the HydraHarp 400 with 1 ps digital resolution and multiple truly parallel channels. These new devices are fundamentally different in design. Instead of operating like a stopwatch, they have independent TDCs for each input channel. If a timing difference is needed (like in classical histogramming) it can be obtained by simple arithmetics in hardware. Figure 7 shows this for the PicoHarp 300 in a block diagram.

Observe the symmetry of the input channels, now both having a CFD. The symmetry as well as the separation of the input channels allows many advanced TCSPC concepts that will be discussed in a separate section further below. For the time being we will first take a look at a TCSPC setup that is fairly independent from the design of the TCSPC electronics used.

Experimental setup for fluorescence decay measurements with TCSPC

Figure 8 shows a typical setup for fluorescence lifetime measurements with TCSPC. The picosecond diode laser (here PDL 800-B) is running on its internal clock (settable at 2.5, 5, 10, 20 or 40 MHz). The driver box is physically separate from the actual laser head, which is attached via a flexible lead. This permits to conveniently place the small laser head anywhere in the optical setup.

The light pulses of typically 50 ps FWHM, are directed at the sample cuvette, possibly via some appropriate optics. A neutral density filter is used to attenuate the light levels to maintain single photon statistics at the detector. Upon excitation, the fluorescent sample will emit light at a longer wavelength than that of the excitation light. The fluorescence light is filtered out against scattered excitation light by means of an optical cut-off filter. Then it is directed to the photon detector, again possibly via some appropriate collection optics, e.g. a microscope objective or just a lens. For timing accuracies of 200 ps FWHM (permitting lifetime measurements even shorter than this via reconvolution) a cheap PMT is sufficient. The electrical signal obtained from the detector (e.g. a small negative pulse of -20 mV) is fed to a pre-amplifier and then to the TCSPC electronics via a standard 50 Ohms coax cable. In this example the complete TCSPC electronics are contained on a single PC-board (TimeHarp 200). Other models are designed as separate boxes connected via USB.

The laser driver also provides the electric sync signal needed for the photon arrival time measurement. This signal (NIM standard, a narrow pulse of -800 mV) is fed to the TCSPC electronics via a standard 50 Ohms coax cable.

Figure 9a shows two fluorescence decay curves obtained with such a simple setup.

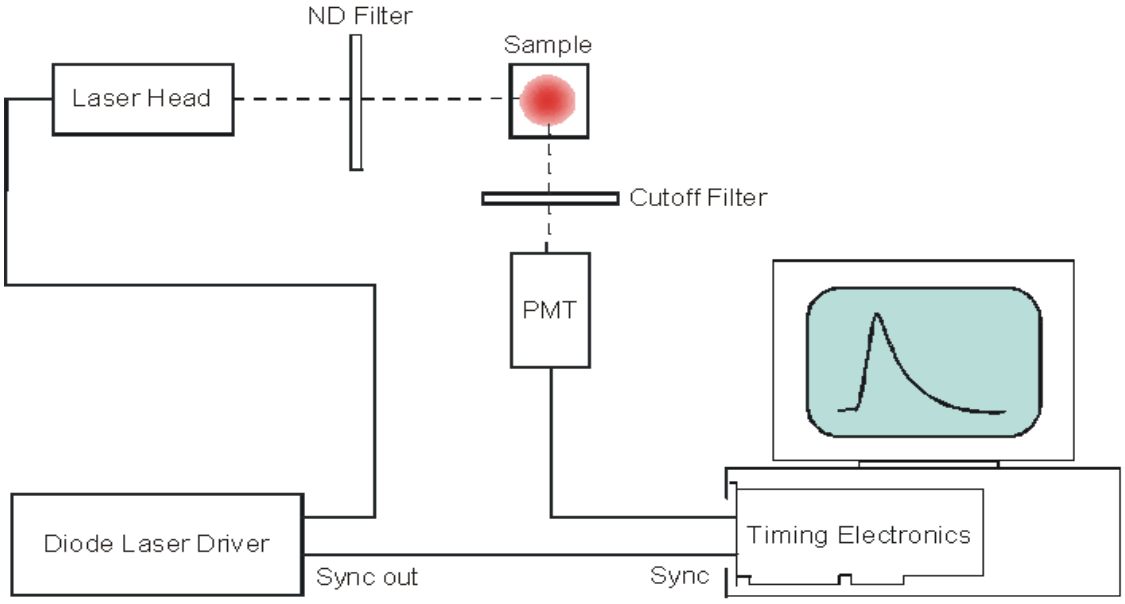

Fig. 8

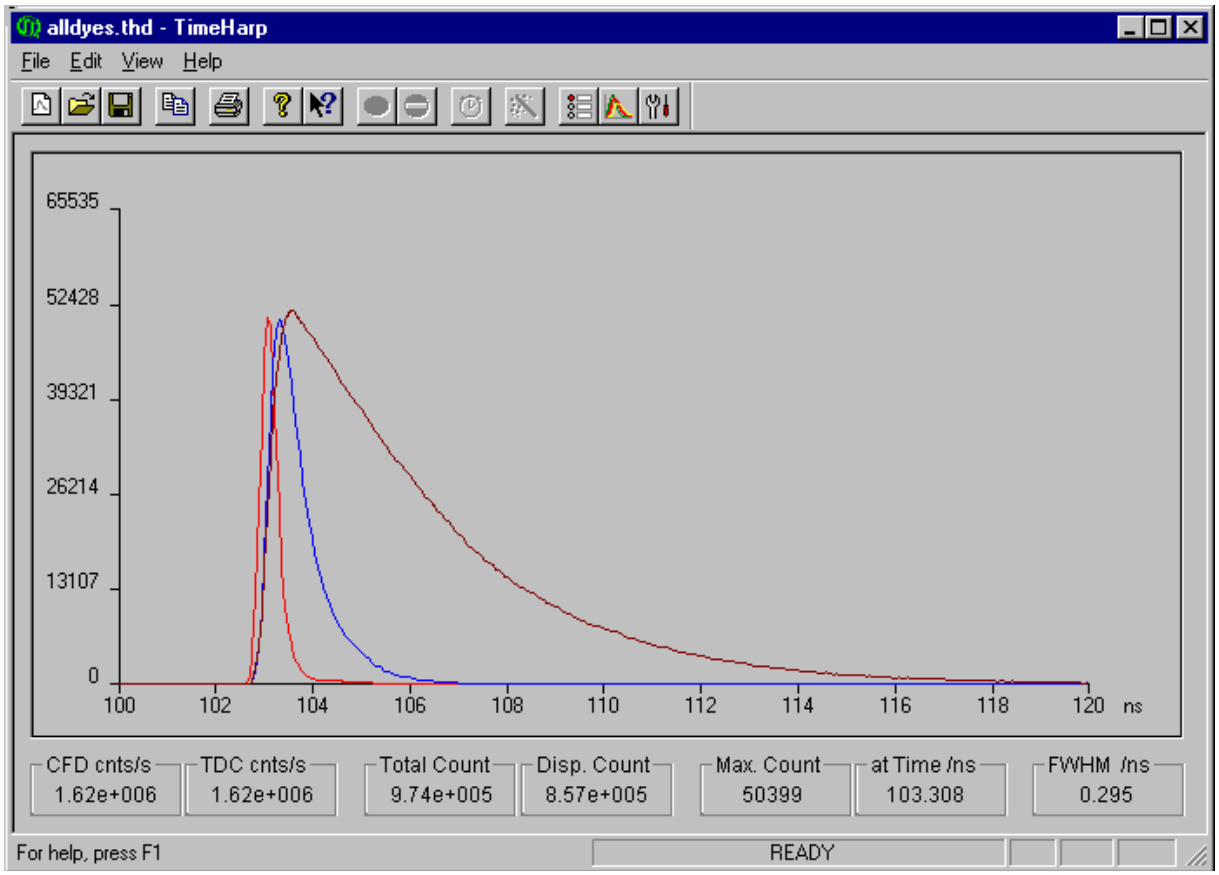
alldyes.thd - TimeHarp
File Edit View Help
65535
52428
39321
26214
13107
0
100 102 104 106 108 110 112 114 116 118 120 ns
CFD cnts/s 1.62e+006
TDC cnts/s 1.62e+006
Total Count 9.74e+005
Disp. Count 8.57e+005
Max. Count 50399
at Time /ns 103.308
FWHM /ns 0.295
For help, press F1
READY

Fig. 9a

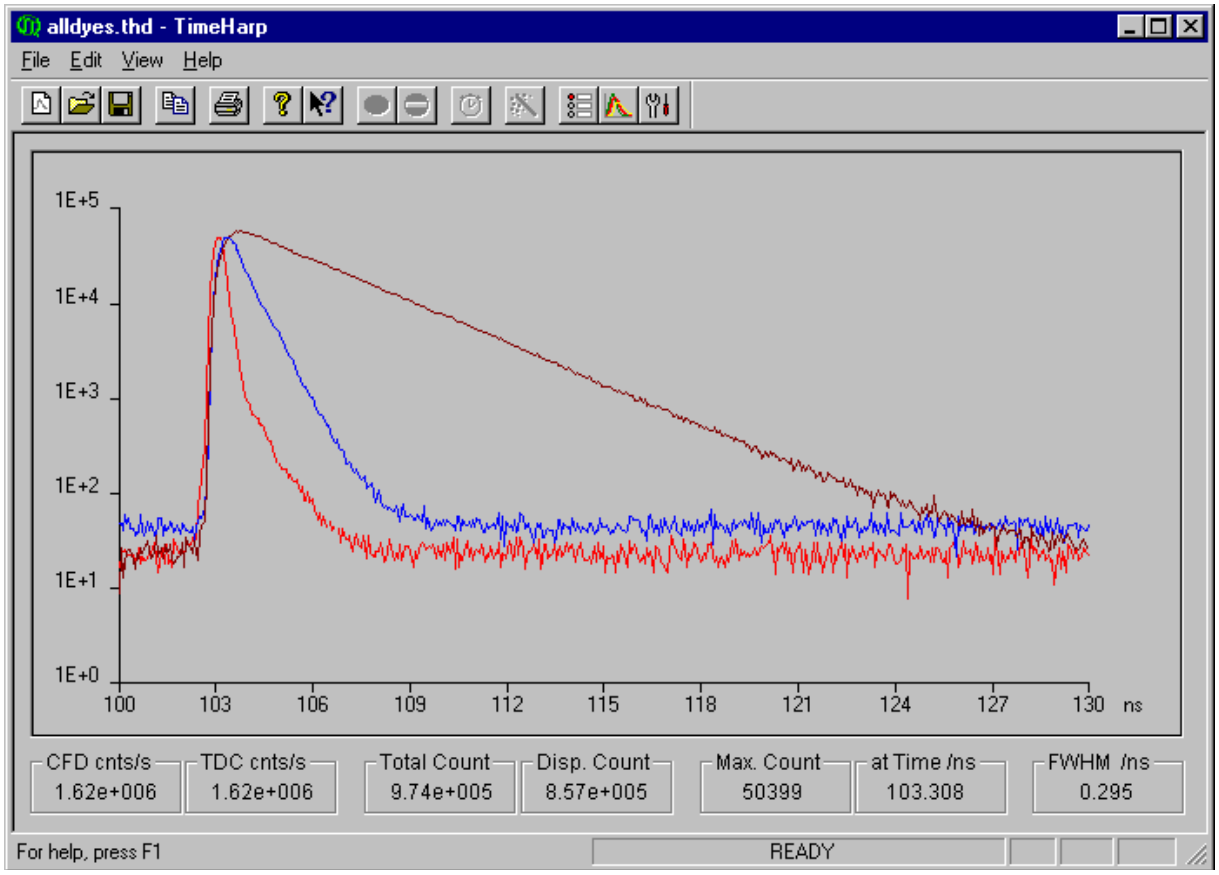
alldyes.thd - TimeHarp
File Edit View Help
1E+5
1E+4
1E+3
1E+2
1E+1
1E+0
100 103 106 109 112 115 118 121 124 127 130 ns
CFD cnts/s 1.62e+006
TDC cnts/s 1.62e+006
Total Count 9.74e+005
Disp. Count 8.57e+005
Max. Count 50399
at Time /ns 103.308
FWHM /ns 0.295
For help, press F1
READY

Fig. 9b

The narrowest curve (red) represents the system IRF, dominated by the detector. The second widest curve (blue) is a fluorescence decay from a solution of Toluidine Blue, a fluorescent dye with relatively short fluorescence lifetime. The widest curve (brown) is from Oxazin 4, another typical fluorescent dye. The excitation source was a PDL 800 at 80 MHz repetition rate.

A second plot in logarithmic scale reveals the nearly perfect exponential nature of the decay curves, as one would expect them (Fig. 9b) Note that this is even without a deconvolution of the relatively broad IRF (300 ps).

The approximate mono-exponential fluorescence lifetime can be obtained from a simple comparison of two points in the exponential display with count rates in the ratio of e:1 (e.g. 27,180:10,000). In this particular experiment this results in a lifetime estimate of 500 ps for Toluidine Blue and 3.1 ns for Oxazin.

For a precise measurement one would perform an iterative reconvolution fit taking into account the IRF. This would result in slightly smaller lifetimes since in this experiment the IRF is nearly as broad as the lifetime to be measured (at least for Toluidine). Nevertheless one can measure lifetimes significantly smaller than the IRF with this method. Additionally the r.m.s. residue from the fit can be used to assess the quality of the fit and thereby the reliability of the lifetime measurement. The FluoFit decay analysis software package from PicoQuant provides this functionality. Of course it is easy to measure long lifetimes with or without reconvolution, since the IRF is of less influence.

Reverse start-stop mode

So far we have always assumed that the time delay measurement should be nicely causal, i.e. the laser pulse causes a photon event and therefore we measure the time delay between laser pulse and subsequent photon event. However, there are practical reasons to give up this convenient concept. The reasons are in the high repetition rates of the typical excitation lasers: Since the time measurement circuit cannot know in advance, whether there will be a fluorescence photon, it would have to start a time measurement upon each laser pulse. Typical conversion times of conventional TCSPC electronics were in the region of 0.5 to 2 µs, and despite significant improvement, they are still 350 ns for the TimeHarp 100/200. Therefore any excitation rate in excess of ~3 MHz would overrun the time measurement circuits. In fact they would most of the time be busy with conversions that never complete, because there is no photon event at all in most cycles. The solution is in the precondition of the single photon counting statistics that must be maintained anyhow. By simply reversing the start and stop signals in the time measurement, the conversion rates are only as high as the actual photon rates generated by the fluorescent sample. These are (and must be) only about 1..5% of the excitation rates and can therefore be handled easily. The consequence of this approach, however, is that the times measured are not those between laser pulse and corresponding photon event but those between photon event and the next laser pulse. This is not too much of a problem, since the laser excitation is periodical and the measured times are directly related to the ones actually needed. As simple as this may sound, there may be yet more problems if the excitation period is very long. This may indeed be of practical relevance, e.g. with flash lamps (<100 kHz). The reverse Start-Stop Principle as explained so far would lead to time delays as long as e.g. 10 ms for 100 kHz excitation rate. These delays are much too long to be measured by conventional TCSPC electronics based on TAC/ADC while the region of interest in this time span (i.e. the actual fluorescence decay) is as short as a few hundred nanoseconds. TDCs generally can measure much longer time spans at high resolution but since there is usually a limited number of histogram bins the system may run into the same limitation. Again, there is a solution: One just has to delay the sync signal corresponding to the true excitation pulse relative to the photon detector signal. This can be done just by a few metres of cable or some sufficient optical path. The detector pulse can thereby 'overtake' the sync pulse and reach the timing electronics first. There it can start the time measurement and the sync pulse arriving later will stop the measurement. This works fine because the cable delays etc. remain constant.

Advanced TCSPC

Historically, the primary goal of TCSPC was the determination of fluorescence lifetimes upon optical excitation by a short light pulse [1,2]. This goal is still important today and therefore has a strong influence on instrument design. However, modifications and extensions of the early designs allow for the recovery of much more information from the detected photons and enable entirely new applications.

Classical TCSPC for fluorescence lifetime measurements only uses the short term difference between excitation and emission. It was soon realized that other aspects of the photon arrival times were of equally great value in the context of single molecule fluorescence detection and spectroscopy. For instance, in single molecule experiments in flow capillaries; an important option is to identify the molecules passing through the detection volume based on their fluorescence lifetime. Each molecule transit is detected as a burst of fluorescence photons. Each time such a transit is detected its fluorescence decay time has to be determined. Also in the area of single molecule detection and spectroscopy, photon coincidence

correlation techniques were adopted to observe antibunching effects that can be used to determine the number of observed emitters as well as the fluorescence lifetime.

Another important method that makes use of temporal photon density fluctuations over a wider time range is Fluorescence Correlation Spectroscopy (FCS). From the fluorescence intensity fluctuations of molecules diffusing through a confocal volume, one can obtain information about the diffusion constant and the number of molecules in the observed volume. This allows sensitive fluorescence assays based on molecule mobility and co-localization. Due to the small numbers of molecules, the photon count rates in FCS are fairly small. Therefore, the only practical way of collecting the data is by means of single photon counting. In order to obtain the time resolution of interest for the diffusion processes, counting with microsecond resolution is required. Hardware correlators for FCS can be implemented very efficiently and recent designs are widely used. However, these instruments are dedicated to correlation with nanosecond resolution at best, and cannot perform picosecond TCSPC.

The requirements of all these analytical techniques based on single photon timing data have much in common. Indeed, all of them can be implemented with the same experimental setup and are based on photon arrival times. A first step towards unified instrumentation for this purpose was a modification of classical TCSPC electronics. The start-stop timing circuitry is used as previously, providing the required picosecond resolution for TCSPC. In order to maintain the information embedded in the temporal patterns of photon arrivals the events are stored as separate records. In addition to that, a coarser timing (time tagging) is performed on each photon event with respect to the start of the experiment. This is called Time-Tagged Time-Resolved (TTTR) data collection [4].

In classical TTTR the different time scales are processed and used rather independently. However, it is of great interest to obtain high resolution timing on the overall scale, i.e. combining coarse and fine timing into one global arrival time figure per event, with picosecond resolution. In a most generic approach, without implicit assumptions on start and stop events, one would ideally just collect precise time stamps of all events of interest (excitation, emission or others) with the highest possible throughput and temporal resolution, and then perform the desired analysis on the original event times. Ideally this would be done on independent channels, so that between channels even dead time effects can be eliminated. These requirements are met by the PicoHarp and HydraHarp TCSPC systems from PicoQuant. Their radically new design enables temporal analysis from picosecond to second time scale, thereby covering almost all dynamic effects of the photophysics of fluorescing molecules. This is achieved by means of independent TDC timing channels allowing picosecond cross-correlations and very high throughput [5,6]. In addition to this enhanced functionality, the new designs eliminate the need for operating in reverse start-stop mode.

PicoQuant TCSPC electronics and system integration

Besides the fast timing electronics for acquisition of e.g. time resolved fluorescence decay profiles, PicoQuant provides pulsed diode lasers and other light sources, bringing the technology to a degree of compactness and ease of use unseen before. This permits the transfer of revolutionary methods from the lab to real life industry applications e.g. in quality control or high throughput screening.

The PicoQuant TCSPC systems contain all components previously accommodated in bulky NIM racks. Nevertheless they outperform conventional systems in many parameters. Due to a versatile design they support many useful measurement modes such as oscilloscope mode for on-the-fly optical alignment or continuous and time tagging modes. Hardware synchronisation pins permit real-time scanning setups with sub-millisecond stepping. DLL libraries as well as demo code are available for custom programming or system integration. A powerful data analysis software for time tagged data is also available.

Apart from supplying stand-alone components, PicoQuant develops complete instruments and supports system integration for specific research applications as well as for OEM needs. Of course we also do not leave the individual user alone with the sometimes tricky task of combining the components for a TCSPC system. We provide help, suggestions and professional consultancy to the individual researcher in the chemistry or biophysics lab as well as to the developer of an industry application. Just call or contact us by email.

References and further reading

[1] Lakowicz, J. R. , Principles of Fluorescence Spectroscopy, 3rd Edition
Springer Science+Business Media, New York, 2006

[2] O'Connor, D.V.O., Phillips, D., Time-correlated Single Photon Counting
Academic Press, London, 1984

[3] O'Connor, D.V.O., Ware, W.R., Andre, J.C.,
"Deconvolution of fluorescence decay curves. A critical comparison of techniques",
J. *Phys. Chem.* **83**, 1333-1343, 1979

[4] Wahl, M., Technical Note on TTTR, PicoQuant, 2004

[5] Wahl M., Rahn H.-J., Gregor I., Erdmann R., Enderlein J.,
"Dead-time optimized time-correlated photon counting instrument with synchronized, independent timing channels", *Review of Scientific Instruments*, **78**, 033106, 2007

[6] Wahl M., Rahn H.-J., Röhlicke T., Kell G., Nettels D., Hillger F., Schuler B., Erdmann R.,
"Scalable time-correlated photon counting system with multiple independent input channels", Review of Scientific Instruments, **79**, 123113, 2008

PicoQuant GmbH
Rudower Chaussee 29 (IGZ)
12489 Berlin
Germany

Phone +49-(0)30-6392-6560
Fax +49-(0)30-6392-6561
Email info@picoquant.com
WWW http://www.picoquant.com

shows that they are indistinguishable at all times (Figure 4.6). On a logarithmic scale, one notices some minor differences at 30–50 ns. However, at 50 ns there are only 3–5 photons per time increment (channel), so that the difference between the two decays is just 1–2 photons. In fact, if one adds the Poisson noise that is inevitably present in photon counting data, the difference between the curves is sevenfold less than the uncertainties due to the Poisson noise.[4] This illustrates that it is difficult to distinguish between some multiexponential functions or, conversely, that it is difficult to recover the actual values of α_i and τ_i for a multiexponential decay. We note that a similar result is obtained from simulations of the FD data. The simulated frequency responses are visually indistinguishable for these two decay laws.

Why is it difficult to resolve multiexponential decays? Comparison of $I_1(t)$ and $I_2(t)$ indicates that the lifetimes and amplitudes are different in each decay law. In fact, this is the problem. For a multiexponential decay, one can vary the lifetime to compensate for the amplitude, or vice versa, and obtain similar intensity decays with different values of α_i and τ_i. In mathematical terms, the values of α_i and τ_i are said to be correlated. The problem of correlated parameters has been described within the framework of general least-squares fitting.[5–7] The unfortunate result is that the ability to determine the precise values of α_i and τ_i is greatly hindered by parameter correlation. There is no way to avoid this problem, except by careful experimentation and conservative interpretation of data.

4.3. TIME-CORRELATED SINGLE-PHOTON COUNTING

At present almost all time-domain measurements are performed using TCSPC. Several comprehensive monographs dealing with TCSPC have appeared.[4,8–10] One book is completely devoted to TCSPC and provides numerous valuable details.[8] While somewhat dated, the insightful monograph of Ware[10] clearly describes the concept of TCSPC, and Ware anticipated many of its present applications. Rather than present a history of the method, we will start with current state-of-the-art instrumentation. These instruments use high-repetition-rate picosecond or femtosecond laser light sources and high-speed MCP PMTs. In later sections we will describe other light sources and detectors.

4.3.A. Principles of TCSPC

The principles of TCSPC can be understood by examination of an instrument schematic (Figure 4.7). The experiment starts with the excitation pulse, which excites the sample and starts the time measurement clock. TCSPC is a digital technique, counting photons which are time-correlated in relation to the excitation pulse. The heart of the method is a time-to-amplitude converter (TAC), which can be considered to be analogous to a fast stopwatch.

The sample is repetitively excited using a pulse light source, often from a laser or flashlamp. Each pulse is optically monitored, by a high-speed photodiode or photomultiplier, to produce a start signal which is used to trigger the voltage ramp of the TAC. The voltage ramp is stopped when the first fluorescence photon from the sample is detected. The TAC provides an output pulse whose voltage is proportional to the time between the start and stop signals. A multichannel analyzer (MCA) converts this voltage to a time channel using an analog-to-digital converter (ADC). Summing over many pulses, the MCA builds up a probability histogram of counts versus time channels. The experiment is continued until one has collected more than 10,000 counts in the peak channel. As will be described below in more detail, there can be no more than one photon detected per 100 laser pulses. Under these conditions, the histogram of photon arrival times represents the intensity decay of the sample.

There are many subtleties in TCSPC which are not obvious at first examination. Why is the photon counting rate limited to one photon per 100 laser pulses? Present electronics for TCSPC only allow detection of the first arriving photon. Once the first photon is detected, the dead time in the electronics prevents detection of another photon resulting from the same excitation pulse. Recall that emission is a random event. Following the excitation pulse, more photons are emitted at early times than at late times. If all could be measured, then the histogram of arrival times would represent the intensity decay. However, if many arrive, and only the first is counted, then the intensity decay is distorted to shorter times. This effect is described in more detail in Section 4.5.F.

Another important feature of TCSPC is the use of the rising edge of the photoelectron pulse for timing. This allows phototubes with nanosecond pulse widths to provide subnanosecond resolution. This is possible because the rising edge of the single photon pulses are usually steeper than one would expect from the time response of the PMT. Also, the use of a constant fraction discriminator provides improved time resolution by removing the variability due to the amplitude of each pulse.

4.3.B. Example of TCSPC Data

Prior to examining the electronic components in more detail, it is valuable to examine the actual data. An intensity

10 Fluorescence Anisotropy

Upon excitation with polarized light, the emission from many samples is also polarized. The extent of polarization of the emission is described in terms of the anisotropy (r). Samples exhibiting nonzero anisotropies are said to display polarized emission. The origin of these phenomena is based on the existence of transition moments for absorption and emission which lie along specific directions within the fluorophore structure. In homogeneous solution the ground-state fluorophores are all randomly oriented. When exposed to polarized light, those fluorophores which have their absorption transition moments oriented along the electric vector of the incident light are preferentially excited. Hence, the excited-state population is not randomly oriented. Instead, there is a somewhat larger number of excited molecules having their transition moments oriented along the electric vector of the polarized exciting light.

Depolarization of the emission can be caused by a number of phenomena, the relative importance of which depends upon the sample under investigation. Rotational diffusion of fluorophores is one common cause of depolarization. The anisotropy measurements reveal the average angular displacement of the fluorophore that occurs between absorption and subsequent emission of a photon. This angular displacement is dependent upon the rate and extent of rotational diffusion during the lifetime of the excited state. These diffusive motions, depend, in turn, upon the viscosity of the solvent and the size and shape of the rotating molecule. For fluorophores in solution, the rotational rate of the fluorophore is dependent upon the viscous drag imposed by the solvent. As a result, a change in solvent viscosity will result in a change in fluorescence anisotropy. For small fluorophores in solutions of low viscosity, the rate of rotational diffusion is typically faster than the rate of emission. Under these conditions, the emission is depolarized and the anisotropy is close to zero.

The dependence of fluorescence anisotropy upon rotational motion has resulted in numerous applications of fluorescence anisotropy measurements in biochemical research. This is because the timescale of rotational diffusion of biomolecules is comparable to the decay time of many fluorophores. For instance, a protein with a molecular weight of 25 kDa can be expected to have a rotational correlation time near 10 ns. This is comparable to the lifetime of many fluorophores when coupled to proteins. Hence, factors which alter the rotational correlation time will also alter the anisotropy. As examples, fluorescence anisotropy measurements have been used to quantify protein denaturation, protein association with other macromolecules, and the internal dynamics of proteins. In addition, the anisotropies of membrane-bound fluorophores have been used to estimate the internal viscosities of membranes and the effects of lipid composition upon the membrane phase-transition temperature.

In this chapter we describe the fundamental theory for steady-state measurements of fluorescence anisotropy and present selected biochemical applications. In the next chapter we will describe the theory and applications of time-resolved anisotropy measurements.

10.1. DEFINITION OF FLUORESCENCE ANISOTROPY

The measurement of fluorescence anisotropy is illustrated in Figure 10.1. The sample is excited with vertically polarized light. The electric vector of the excitation light is oriented parallel to the vertical or z-axis. One then measures the intensity of the emission through a polarizer. When the emission polarizer is oriented parallel ($\parallel$) to the direction of the polarized excitation, the observed intensity is called $I_{\parallel}$. Likewise, when the polarizer is perpendicular ($\perp$) to the excitation, the intensity is called $I_{\perp}$. These values are used to calculate the anisotropy[1]:

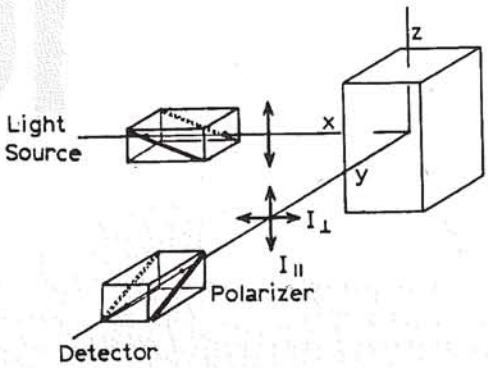

Figure 10.1. Schematic diagram for measurement of fluorescence anisotropies.

$$r = \frac{I_{\parallel} - I_{\perp}}{I_{\parallel} + 2I_{\perp}} \qquad [10.1]$$

The anisotropy is a dimensionless quantity which is independent of the total intensity of the sample. This is because the difference $(I_{\parallel} - I_{\perp})$ is normalized by the total intensity, which is $I_T = I_{\parallel} + 2I_{\perp}$.

In earlier publications one frequently encounters the term polarization, which is given by

$$P = \frac{I_{\parallel} - I_{\perp}}{I_{\parallel} + I_{\perp}} \qquad [10.2]$$

The polarization and anisotropy values can be interchanged using

$$P = \frac{3r}{2 + r} \qquad [10.3]$$

$$r = \frac{2P}{3 - P} \qquad [10.4]$$

Although there is nothing incorrect about the notion of polarization, its use should be discouraged. Anisotropy is preferred because most theoretical expressions are considerably simpler when expressed in terms of this parameter, an observation first made by Alexander Jabłoński.[1] As an example of this simplification, consider a mixture of fluorophores, each with polarization P_i and a fractional fluorescence intensity f_i. The polarization of this mixture $(\overline{P})$ is given by[2]

$$\left(\frac{1}{P} - \frac{1}{3}\right)^{-1} = \sum_i \frac{f_i}{\left(\frac{1}{P_i} - \frac{1}{3}\right)} \qquad [10.5]$$

In contrast, the average anisotropy $(\overline{r})$ is given by

$$\overline{r} = \sum_i f_i r_i \qquad [10.6]$$

where the r_i indicate the anisotropies of the individual species. The latter expression is clearly preferable. Furthermore, following pulsed excitation, the decay of fluorescence anisotropy $[r(t)]$ of a sphere is given by

$$r(t) = r_0 e^{-t/\theta} \qquad [10.7]$$

where r_0 is the anisotropy at $t = 0$, and θ is the rotational correlation time of the sphere. The decay of polarization is not a single exponential, even for a spherical molecule.

Suppose that the light observed through the emission polarizer is completely polarized. Then $I_{\perp} = 0$, and $P = r = 1.0$. This value can be observed for scattered light from an optically dilute scatterer. Completely polarized emission is never observed for fluorescence from homogeneous unoriented samples. The measured values of P or r are smaller due to the angular dependence of photoselection (Section 10.2). Completely polarized emission can be observed for oriented samples.

Now suppose that the emission is completely depolarized. In this case, $I_{\parallel} = I_{\perp}$ and $P = r = 0$. However, it is important to note that P and r are not equal for intermediate values. For the moment, we have assumed that these intensities could be measured without artifacts due to the polarizing properties of the optical components, especially the emission monochromator (Section 2.3.B). In Section 10.4 we will describe methods to correct for such interference.

10.1.A. Origin of the Definitions of Polarization and Anisotropy

One may wonder why two widely used measures exist for the same phenomenon. Both P and r have a rational origin. Consider partially polarized light traveling along the x-axis (Figure 10.2), and assume that one measures the intensities I_z and I_y with the detector and polarizer positioned on the x-axis. The polarization of this light is defined as the fraction of the light that is linearly polarized. Specifically,

$$P = \frac{p}{p + n} \qquad [10.8]$$

where p is the intensity of the polarized component, and n is the intensity of the natural component. The intensity of the natural component is given by $n = 2I_y$. The remaining intensity is the polarized component, which is given by $p = I_z - I_y$. For vertically polarized excitation, $I_z = I_{\parallel}$ and $I_y = I_{\perp}$.

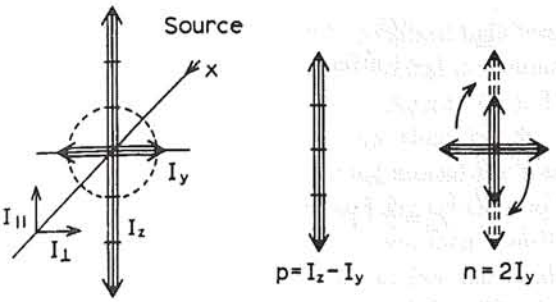

Figure 10.2. Polarization of a ray of light.

Substitution into Eq. [10.8] yields Eq. [10.2], which is the standard definition for polarization.

The anisotropy (r) of a light source is defined as the ratio of the polarized component to the total intensity (I_T),

$$r = \frac{I_z - I_y}{I_x + I_y + I_z} = \frac{I_z - I_y}{I_T} \qquad [10.9]$$

When the excitation is polarized along the z-axis, dipolar radiation from the fluorophores is also symmetric around the z-axis. Hence, $I_x = I_y$. Recalling that $I_y = I_\perp$ and $I_z = I_{||}$, one obtains Eq. [10.1].

The polarization is an appropriate parameter for describing a light source when a light ray is directed along a particular axis. In this case, $p + n$ is the total intensity, and P is the ratio of the excess intensity along the z-axis divided by the total intensity. In contrast, the radiation emitted by a fluorophore is symmetrically distributed about the z-axis.

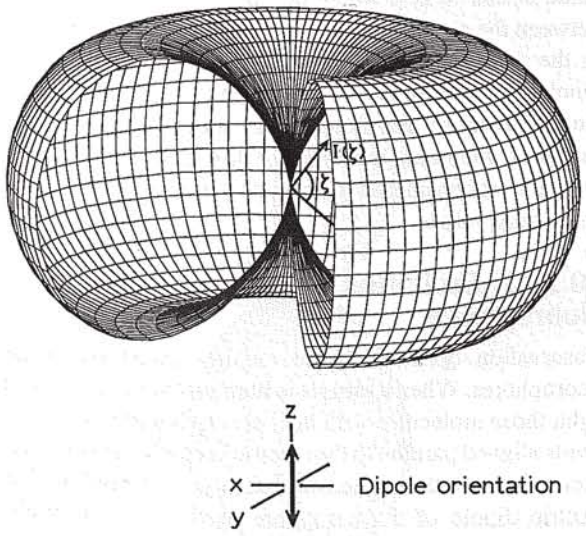

Figure 10.3. Radiating dipole in a coordinate system. The dipole is oriented along the z-axis, and the intensity $I(\zeta)$ of the emission in any direction is proportional to $\cos^2 \zeta$, where ζ is the angle from the x–y plane.

This distribution of radiated intensity is shown in Figure 10.3 for a dipole oriented along the z-axis. The intensity of the radiated light is proportional to $\cos^2 \zeta$, where ζ is the angle above or below the x–y plane. It is for this reason that, for excitation polarized along the z-axis, the total intensity is not given by $I_{||} + I_\perp$, but rather by $I_T = I_{||} + 2\,I_\perp$ (Section 10.4.F). Hence, the anisotropy is the ratio of the excess intensity that is parallel to the z-axis to the total intensity. It is interesting to notice that a dipole oriented along the z-axis does not radiate along this axis and cannot be observed with a detector on the z-axis.

10.2. THEORY FOR ANISOTROPY

The theory for fluorescence anisotropy can be derived by consideration of a single molecule.[3] Assume for the moment that the absorption and emission transition moments are parallel. This is nearly true for the membrane probe DPH. Assume that this single molecule is oriented with angles θ relative to the z-axis and ϕ relative to the y-axis (Figure 10.4). Of course, the ground-state DPH molecules will be randomly oriented in an isotropic solvent. Our goal is to calculate the anisotropy that would be observed for this oriented molecule in the absence of rotational diffusion. The conditions of parallel dipoles, immobility, and random ground-state orientation simplify the derivation.

It is known that fluorescing fluorophores behave like radiating dipoles.[4] The intensity of light radiated from a

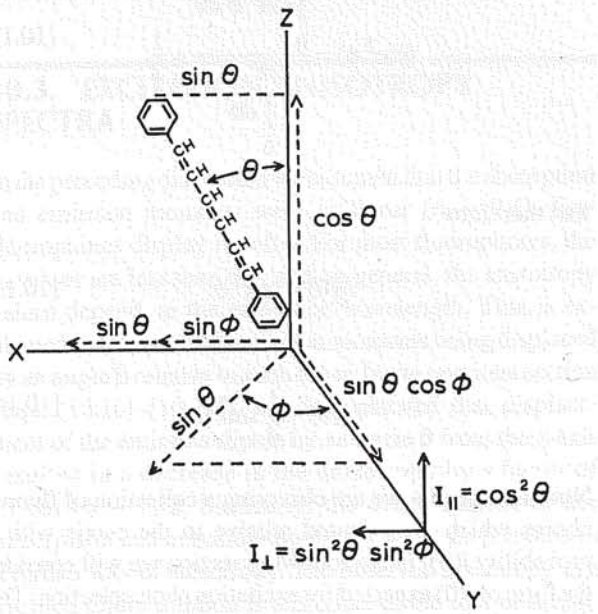

Figure 10.4. Emission intensities for a single fluorophore in a coordinate system.

dipole is proportional to the square of its vector projected onto the axis of observation. One can also reason that the emission is polarized along the transition moment. The intensity observed through a polarizer is proportional to the square of the projection of the electric field of the radiating dipole onto the transmission axis of the polarizer. These projections are given by

$$I_{\parallel}(\theta, \phi) = \cos^2 \theta \qquad [10.10]$$

$$I_{\perp}(\theta, \phi) = \sin^2 \theta \sin^2 \phi \qquad [10.11]$$

In an actual experiment the solution will contain many fluorophores with a random distribution. The anisotropy is calculated by performing the appropriate average based on excitation photoselection and how the selected molecules contribute to the measured intensity. First, consider excitation polarized along the z-axis. Such excitation must excite all molecules having an angle ϕ with respect to the y-axis with equal probability. That is, the population of excited fluorophores will be symmetrically distributed around the z-axis. Any experimentally accessible population of molecules will be oriented with values of ϕ from 0 to 2π with equal probability. Hence, we can eliminate the ϕ dependence in Eq. [10.11]. The average value of $\sin^2 \phi$ is given by

$$\langle \sin^2 \phi \rangle = \frac{\int_0^{2\pi} \sin^2 \phi \, d\phi}{\int_0^{2\pi} d\phi} = \frac{1}{2} \qquad [10.12]$$

and therefore

$$I_{\parallel}(\theta) = \cos^2 \theta \qquad [10.13]$$

$$I_{\perp}(\theta) = \frac{1}{2} \sin^2 \theta \qquad [10.14]$$

Now assume that we are observing a collection of fluorophores which are oriented relative to the z-axis with a probability $f(\theta)$. In the following section we will consider the form of $f(\theta)$ expected for excitation photoselection. The measured fluorescence intensities for this collection of molecules are

$$I_{\parallel} = \int_0^{\pi/2} f(\theta) \cos^2 \theta \, d\theta = k \langle \cos^2 \theta \rangle \qquad [10.15]$$

$$I_{\perp} = \frac{1}{2} \int_0^{\pi/2} f(\theta) \sin^2 \theta \, d\theta \, \frac{k}{2} \langle \sin^2 \theta \rangle \qquad [10.16]$$

where $f(\theta)\, d\theta$ is the probability that a fluorophore is oriented between θ and $\theta + d\theta$, and k is an instrumental constant. Using Eq. [10.11] and the identity $\sin^2 \theta = 1 - \cos^2 \theta$, one finds that

$$r = \frac{3\langle \cos^2 \theta \rangle - 1}{2} \qquad [10.17]$$

Hence, the anisotropy is determined by the average value of $\cos^2 \theta$, where θ is the angle of the emission dipole relative to the z-axis. This is because the observed intensities $I_{\parallel}$ and $I_{\perp}$ are proportional to the square of the projection of the individual transition moments onto the x- and the z-axis (Figure 10.4).

It is instructive to consider the relationship between r and θ. For a single fluorophore oriented along the z-axis, with collinear transitions, $\theta = 0$ and $r = 1.0$. However, it is not possible to obtain a perfectly oriented excited-state population with optical excitation of homogeneous solutions. Hence, the anisotropies are always less than 1.0. Complete loss of anisotropy is equivalent to $\theta = 54.7°$. This does not mean that each fluorophore is oriented at 54.7° or has rotated through 54.7°. Rather, it means that the average value of $\cos^2 \theta$ is $\frac{1}{3}$, where θ is the angular displacement between the excitation and emission moments. Recall that in the derivation of Eq. [10.17] we assumed that these dipoles were collinear. A slightly more complex expression is necessary for almost all fluorophores because the transition moments are rarely collinear. In addition, we have not yet considered the effects of photoselection on the anisotropy values.

10.2.A. Excitation Photoselection of Fluorophores

Observation of fluorescence requires excitation of the fluorophores. When a sample is illuminated with polarized light, those molecules with their absorption transition moments aligned parallel to the electric vector of the polarized excitation have the highest probability of absorption. The electric dipole of a fluorophore need not be precisely aligned with the z-axis to absorb light polarized along this axis. The probability of absorption is proportional to $\cos^2 \theta$, where θ is the angle the absorption dipole makes with

the z-axis.[3] Hence, excitation with polarized light results in a population of excited fluorophores that is symmetrically distributed around the z-axis (Figure 10.5). This phenomenon is called photoselection. Note that the excited-state population is symmetrical around the z-axis. Most of the excited fluorophores are aligned close to the z-axis, and very few fluorophores have their transition moments oriented in the x–y plane. For the random ground-state distribution, which must exist in a disordered solution, the number of molecules at an angle between θ and $\theta + d\theta$ is proportional to $\sin\theta\, d\theta$. This quantity is proportional to the surface area on a sphere within the angles θ and $\theta + d\theta$. Hence, the distribution of molecules excited by vertically polarized light is given by

$$f(\theta)\, d\theta = \cos^2\theta \sin\theta\, d\theta \qquad [10.18]$$

The probability distribution given by Eq. [10.18] determines the maximum photoselection that can be obtained using one-photon excitation of an isotropic solution. More highly oriented populations can be obtained using multiphoton excitation.[5] Recall that the anisotropy is a simple function of $\langle\cos^2\theta\rangle$ (Eq. [10.17]), so calculation of $\langle\cos^2\theta\rangle$ allows calculation of the anisotropy.

For collinear absorption and emission dipoles, the maximum value of $\langle\cos^2\theta\rangle$ is given by

$$\langle\cos^2\theta\rangle = \frac{\int_0^{\pi/2} \cos^2\theta\, f(\theta)\, d\theta}{\int_0^{\pi/2} f(\theta)\, d\theta} \qquad [10.19]$$

Substitution of Eq. [10.18] into Eq. [10.19] yields $\langle\cos^2\theta\rangle = \frac{3}{5}$. Recalling Eq. [10.17], one finds a maximum anisotropy of 0.4. This is the value which is observed when the absorption and emission dipoles are collinear, and when there are no processes which result in depolarization. Under these conditions, the excited-state population is preferentially oriented along the z-axis (Figure 10.5), and the value of $I_\perp$ is one-third the value of $I_\parallel$ ($I_\parallel = 3I_\perp$). We note that this value ($r = 0.4$) is considerably smaller than that possible for a single fluorophore oriented along the z-axis ($r = 1.0$).

It is important to remember that there are other possible origins for polarized light. These include reflections and light scattered by the sample. For a dilute scattering solution, the anisotropy is close to 1.0. Scattered light can interfere with anisotropy measurements. If the measured anisotropy for a randomly oriented sample is greater than 0.4, one can confidently infer the presence of scattered light in addition to fluorescence. The maximum anisotropy of 0.4 for collinear absorption and emission dipoles is a consequence of the $\cos^2\theta$ probability of light absorption. Anisotropy values can exceed 0.4 for multiphoton excitation (Section 10.13).

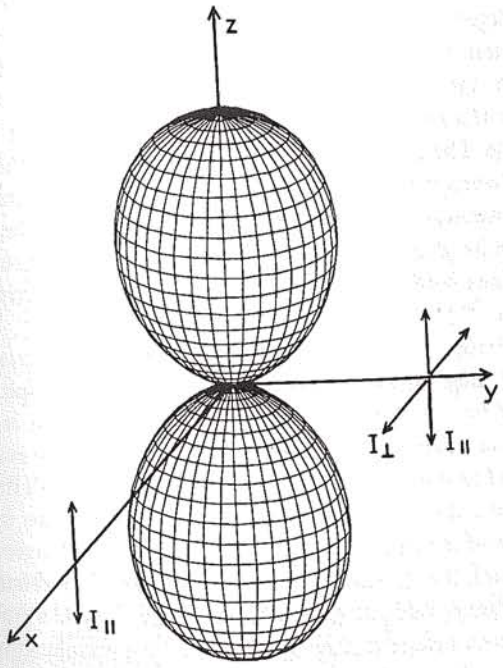

Figure 10.5. Excited-state distribution for immobile fluorophores with $r_0 = 0.4$.

10.3. EXCITATION ANISOTROPY SPECTRA

In the preceding discussion we assumed that the absorption and emission moments were collinear ($r_0 = 0.4$). Few fluorophores display $r_0 = 0.4$. For most fluorophores, the r_0 values are less than 0.4, and, in general, the anisotropy values depend on the excitation wavelength. This is explained in terms of the transition moments being displaced by an angle β relative to each other. In the previous section (Eqs. [10.10]–[10.17]), we demonstrated that displacement of the emission dipole by an angle θ from the z-axis resulted in a decrease in the anisotropy by a factor of $(3\cos^2\theta - 1)/2$. Similarly, the displacement of the absorption and emission dipoles by an angle β results in a further loss of anisotropy. The observed anisotropy in a vitrified dilute solution is a product of the loss of anisotropy due to photoselection (resulting in a reduction of the anisotropy by a factor of $\frac{2}{5}$) and that due to the angular

11

Time-Dependent Anisotropy Decays

In the preceding chapter we described the measurement and interpretation of steady-state fluorescence anisotropies. These values are measured using continuous illumination and represent an average of the anisotropy decay over the intensity decay. Measurement of steady-state anisotropies is simple, but interpretation of the steady-state anisotropies usually depends on an assumed form for the anisotropy decay, which is not directly observed in the experiment. Additional information is available if one measures the time-dependent anisotropy, that is, the values of $r(t)$ following pulsed excitation. The form of the anisotropy decay depends on the size, shape, and flexibility of the labeled molecule, and the data can be compared with the decays calculated from various molecular models. Anisotropy decays can be obtained using the TD or the FD method.

It is valuable to understand the factors which affect the anisotropy decays. For a spherical molecule, the anisotropy is expected to decay with a single rotational correlation time (θ). Perhaps the most frequent interpretation of the correlation time is in terms of the overall rotational correlation time of a protein. The measured values of θ can compare with the value predicted for a hydrated sphere of equivalent molecular weight (Eq. [10.52]). However, numerous factors can result in multiexponential anisotropy decays. Multiexponential anisotropy decays are expected for nonspherical fluorophores or proteins. In this case the correlation times are determined by the rates of rotation about the various molecular axes. Anisotropy decays can be used to estimate the shapes of proteins.

In addition to being affected by shape, anisotropy decays are affected by the segmental flexibility of the macromolecule. For instance, tryptophan anisotropy decays of proteins frequently display correlation times that are too short to be due to rotational diffusion of the whole macromolecule. These short-correlation-time components are often due to independent motions of the tryptophan residue within the protein. Measurements of these components have been widely used to understand the internal dynamics of proteins. Anisotropy decays can also be affected by RET between molecules of the same type of fluorophore, that is, depolarization due to homotransfer.

Anisotropy decays of membrane-bound probes have been particularly informative. Membrane-bound probes often display unusual behavior, whereby the anisotropies do not decay to zero. This behavior occurs because, in contrast to probes in isotropic solutions, probes in membranes do not rotate freely. The extent of rotation is often limited by the anisotropic environment of a membrane. The nonzero anisotropies at long times have been interpreted in terms of the order parameters of the membrane. In this chapter we present examples of simple and complex anisotropy decays to illustrate the wealth of information available from measurements of time-dependent anisotropies. In the following chapter we describe more advanced concepts in anisotropy decay analysis.

11.1. ANALYSIS OF TIME-DOMAIN ANISOTROPY DECAYS

Suppose that a fluorophore is excited with a pulse of vertically polarized light and that it rotates with a single correlation time. The anisotropy decay is determined by measuring the decay of the vertically (||) and horizontally ($\perp$) polarized components of the emission. If the absorption and emission transition moments are collinear, the time-zero anisotropy is 0.4. In this case the initial intensity of the parallel component is threefold larger than that of the perpendicular component (Figure 11.1, left). Assuming that the fundamental anisotropy is greater than zero ($r_0 > 0$), the vertically polarized excitation pulse results in an initial population of fluorophores that is enriched in the parallel orientation. The decay of the difference between $I_{\parallel}(t)$ and $I_{\perp}(t)$, when properly normalized by the total intensity, is the anisotropy decay (Figure 11.1, right).

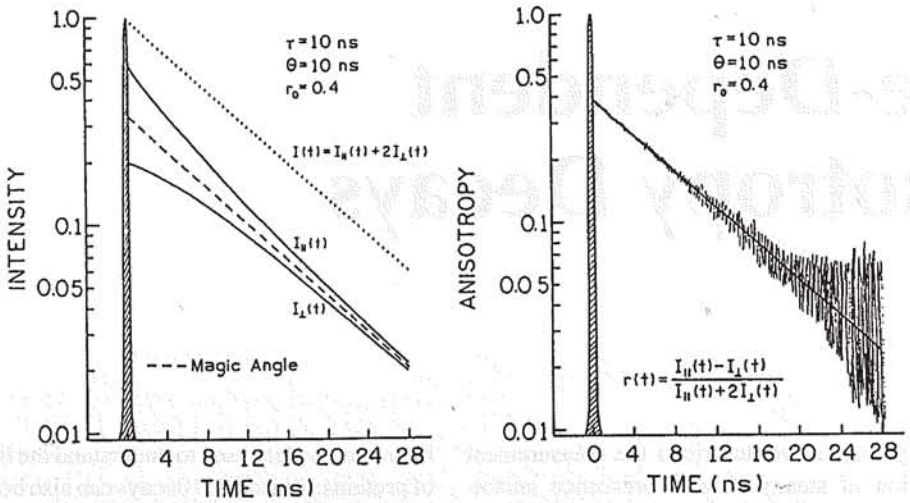

Figure 11.1. Time-dependent polarized decays (*left*) and the calculated anisotropy decay (*right*). From Ref. 1.

Examination of the left panel in Figure 11.1 reveals that the parallel component initially decays more rapidly than the horizontal component. This occurs because the vertically oriented fluorophores are decaying by two processes, the intensity decay with decay time τ and rotation out of the vertical orientation with a correlation time θ. The horizontal component initially decays more slowly because it is repopulated by rotation from the excess vertically oriented population.

Interpretation of anisotropy decays is best understood in terms of the individual components. The decays of the parallel ($\|$) and perpendicular ($\perp$) components of the emission are given by

$$I_{\|}(t) = \frac{1}{3} I(t)[1 + 2r(t)] \qquad [11.1]$$

$$I_{\perp}(t) = \frac{1}{3} I(t)[1 - r(t)] \qquad [11.2]$$

where $r(t)$ is the time-resolved anisotropy. Generally, $r(t)$ can be described as a multiexponential decay,

$$r(t) = r_0 \sum_j g_j \exp(-t/\theta_j) = \sum_j r_{0j} \exp(-t/\theta_j) \qquad [11.3]$$

where $r_0 = \Sigma_j r_{0j}$ is the limiting anisotropy in the absence of rotational diffusion, the θ_j are the individual correlation times, and the g_j are the associated fractional amplitudes in the anisotropy decay ($\Sigma g_j = 1.0$). Depending on the circumstances, r_0 may be a known parameter, perhaps from a frozen solution measurement. Alternatively, all the amplitudes (r_{0j}) can be considered to be experimental variables. As shown in the previous chapter, the total intensity for a sample is given by $I_T = I_{\|} + 2I_{\perp}$. Similarly, the total (rotation-free) intensity decay is given by

$$I(t) = I_{\|}(t) + 2I_{\perp}(t) \qquad [11.4]$$

In the time domain, one measures the time-dependent decays of the polarized components of the emission (Eqs. [11.1] and [11.2]). The polarized intensity decays are used to calculate the time-dependent anisotropy,

$$r(t) = \frac{I_{\|}(t) - I_{\perp}(t)}{I_{\|}(t) + 2I_{\perp}(t)} \qquad [11.5]$$

The time-dependent anisotropy decay is then analyzed to determine which model is most consistent with the data.

The experimental procedures and the form of the data are different for FD measurements of the anisotropy decays.[2] The sample is excited with amplitude-modulated light which is vertically polarized (Figure 11.2). As for the TD measurements, the emission is observed through a polarizer, which is rotated between the parallel and the perpendicular orientations. In the frequency domain, there are two observable quantities which characterize the anisotropy decay. These are the phase shift Δ_ω, at the modulation frequency ω, between the perpendicular ($\phi_\perp$) and parallel ($\phi_{\|}$) components of the emission,

$$\Delta_\omega = \phi_\perp - \phi_{\|} \qquad [11.6]$$

and the ratio of the parallel ($m_{\|}$) and the perpendicular ($m_\perp$) components of the modulated emission,

BIOCHEMISTRY AND MOLECULAR BIOLOGY EDUCATION
Vol. 31, No. 5, pp. 319–322, 2003

Laboratory Exercises

Tästä kannattaa silmäillä johdanto tuohon materials ja methodsiin asti.

Determination of the Molecular Size of BSA by Fluorescence Anisotropy*

Received for publication, January 16, 2003, and in revised form, May 29, 2003

F. Luis González Flecha and Valeria Levi‡

From the Instituto de Química y Fisicoquímica Biológicas, Departamento de Química Biológica, Facultad de Farmacia y Bioquímica, Universidad de Buenos Aires, Argentina

This work describes a laboratory experiment to illustrate the usefulness of fluorescence anisotropy in the field of biophysics. Fluorescence anisotropy of dansyl-labeled BSA was determined in media of increasing glycerol concentrations. The Perrin equation was fitted to the experimental data, obtaining the molecular volume of the protein. The simplicity of the experiment and data analysis helped the students to focus on the relationship between probe anisotropy and rotational diffusion. Additionally, this laboratory exercise has the advantage of using a protein and a probe that are inexpensive and very common in many laboratories.

Keywords: BSA, fluorescence anisotropy, molecular size.

Light is an electromagnetic wave that can be described as oscillating electric and magnetic fields perpendicular to each other. The electric field vector can be represented in an X-Y plane perpendicular to the direction of propagation. When the X and Y components oscillate at the same phase, the result is an oscillation in a defined orientation that depends on the relative amplitude of each component. In this condition, the light is called linearly polarized [1].

Molecular electronic transitions are described in quantum mechanics by vectors in the physical space denoted as transition moments. According to this description, the probability of light absorption by molecules irradiated with linearly polarized light will be proportional to the component of the absorption moment parallel to the polarization axis of the incident radiation [2]. This phenomenon is known as photoselection (Scheme I).

As a consequence of photoselection, the resulting emitted light will also be polarized in a plane defined by the emission moment. To characterize the polarized state of the emitted light, it was defined as a parameter called fluorescence anisotropy (r),

$$r = \frac{I_{//} - I_{\perp}}{I_T} = \frac{I_{//} - I_{\perp}}{I_{//} + 2 \cdot I_{\perp}} \qquad \text{(Eq. 1)}$$

where $I_{//}$ and $I_{\perp}$ are the components of the fluorescence intensity that are parallel and perpendicular to the electric vector of the excitation light, and I_T is the total fluorescence intensity [3].

In the absence of diffusion, the anisotropy is given by the relative orientation of the excitation and emission moments of the fluorophore, taking values between −0.2 (perpendicular transition moments) and 0.4 (parallel transition moments). In solution, the excited molecules can rotate, thereby changing their orientation (Scheme II). The angle θ between the average orientation of the molecules at a given time with respect to the original orientation depends on the time, the temperature, the solvent properties, and the size and shape of the molecule. This process, known as rotational diffusion, can be characterized by a parameter called rotational correlational time (ϕ), defined as the time after which $\cos\,\theta = e^{-1}$ [4].

In 1926, Perrin proposed that rotational diffusion contributes to depolarizing the emitted light and postulated the following relationship to explain the dependence of the anisotropy with the rotational diffusion process [5],

$$r = \frac{r_0}{1 + \tau/\phi} \qquad \text{(Eq. 2)}$$

where r_o is the anisotropy in the absence of diffusion, τ is the fluorescence lifetime, and ϕ is the rotational correlation time of the fluorophore. In a fluorescent conjugate that behaves in solution as a rigid rotator, the parameters r_o and τ depend on the photophysical properties of the fluorophore, whereas ϕ depends mainly on the size and shape of the macromolecule [4].

Equation 2 predicts that, when $\tau \ll \phi$, the particle would almost not rotate at all during the lifetime of the fluorophore, and r approaches the anisotropy measured in the absence of diffusion, *i.e.* r_o. On the other hand, when $\tau \gg \phi$, the emission dipoles of the molecule become randomly distributed as a consequence of the rotational diffusion, and r approaches zero. The anisotropy will be sensitive to factors affecting the rotational motions when $\tau \cong \phi$.

* This work was partially supported by the University of Buenos Aires (UBACYT B612 and FFyB AT 5357).

‡ To whom correspondence should be addressed: E-mail: vlevi@uiuc.edu (current address: Department of Physics, University of Illinois at Urbana-Champaign).

Considering spherical particles rotating with small angular velocities, the rotational correlation time can be expressed by the Stokes-Einstein-Debye equation [5],

Tätä käytetään

$$\phi = \frac{\eta \cdot V}{k \cdot T} \qquad \text{(Eq. 3)}$$

where η is the solvent viscosity coefficient, k is the Boltzman constant, T is temperature, and V is the volume of the rotating particle. This equation is based on classical hydrodynamics and requires the hypothesis of a continuous and homogeneous solvent. Some doubt may be cast on this assumption in the case of molecules that do not differ greatly in size from the molecules of solvent. However, this approximation appears to be valid for proteins [4].

For nonspherical molecules, more than one rotational correlation time is needed to describe their rotational motion. However, if the molecule is slightly asymmetrical, Equation 2 can be applied and ϕ will represent a mean value of the principal relaxation times of the rotation [6]. In this case, the parameter V in Equation 3 will be the volume of a hydrodynamically equivalent sphere.

Combining Equation 3 with Equation 2 results in

$$r = \frac{r_0}{1 + \frac{\tau \cdot k \cdot T}{\eta \cdot V}} = \frac{\eta \cdot r_0}{\eta + c} \qquad \text{(Eq. 4)}$$

where c is a fitting coefficient that includes the constant terms in the denominator and corresponds to the solvent viscosity at which the steady state anisotropy is reduced at half of the limit value.

Equation 4 shows that fluorescence anisotropy depends on the volume of the rotating particle. This relationship constitutes the basis of many applications of this technique to the study of biological processes involving volume changes (*e.g.* interactions among macromolecules [7], conformational changes [8], etc.). In this work, we show a simple experiment that uses fluorescence anisotropy to determine the molecular size of a protein.

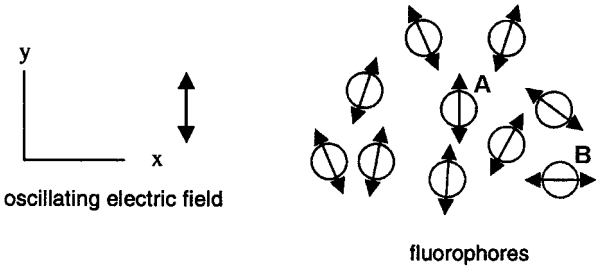

SCHEME 1. **Photoselection of fluorophores.** The electric vector of the excitation light and the absorption dipoles of randomly distributed fluorophores are shown. Molecules A and B exhibit maximal and no absorption of light, respectively.

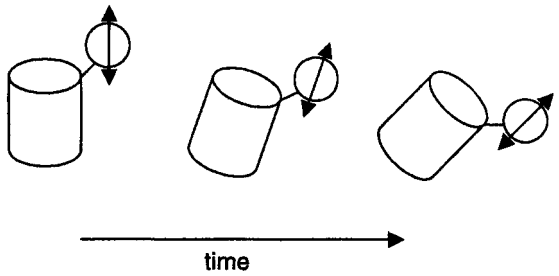

SCHEME 2. **Rotational diffusion of a labeled molecule.**

MATERIALS AND METHODS

Materials—BSA (catalog no. A-7906) and dansyl-chloride (catalog no. D-2625) were obtained from Sigma Chemical Co. All other chemicals used in this work were of analytical grade.

Labeling with Dansyl-chloride—BSA was labeled by the students in a previous laboratory class [9]. Briefly, they incubated 300 μM dansyl chloride (previously dissolved in a small volume of dimethylformamide) and 300 μM BSA in 10 mM morpholinopropane-sulfonic acid (MOPS)-K (pH 8.4 at 25 °C) for 1.5 h at 25 °C in the dark, with continuous stirring. The reaction was stopped by the addition of 10 mM Tris, and the sample was exhaustively dialyzed against 10 mM Tris-HCl (pH 7.4 at 20 °C). The stoichiometry of labeling was 0.95 [9].

Dansyl-Tris was obtained by incubating, in the dark, 300 μM of the fluorescent probe in 10 mM Tris-HCl (pH 8.4) at 25 °C for 1.5 h. After that, the sample pH was adjusted to 7.4 at 20 °C with 1 M HCl.

Preparation of the Samples—A glycerol solution (25% p/p) was prepared by mixing 10 g of glycerol (87%) with 24.8 g of H_2O. Dansyl-BSA was diluted up to 30 μM in 10 mM Tris-HCl pH 7.4 at 20 °C and increasing quantities of glycerol by following the procedure detailed in Table I. Each sample was prepared in duplicate. Because the protein and buffer concentrations are very low, sample viscosities can be calculated from the glycerol concentration. For this task, students plotted the data of viscosity of glycerol-water solutions as a function of their concentrations (*Handbook of Chemistry and Physics*, www.hbcpnetbase.com) and fitted a second-order polynomial function to these data (Fig. 1). They then calculated the viscosities of the BSA samples using

TABLE I
Preparation of the samples

Sample no.	Final glycerol concentration	BSA (300 μM)	Tris-HCl (1 M, pH 7.4 at 20 °C)	Glycerol (25 % p/p)	H_2O
	% p/p	μl	μl	μl	μl
1	0	300	27	0	2673
2	2	300	27	240	2433
3	4	300	27	480	2193
4	6	300	27	720	1953
5	8	300	27	960	1713
6	10	300	27	1200	1473
7	12	300	27	1440	1233
8	14	300	27	1680	993
9	16	300	27	1920	753
10	18	300	27	2160	513
11	20	300	27	2400	273
12	22	300	27	2640	33

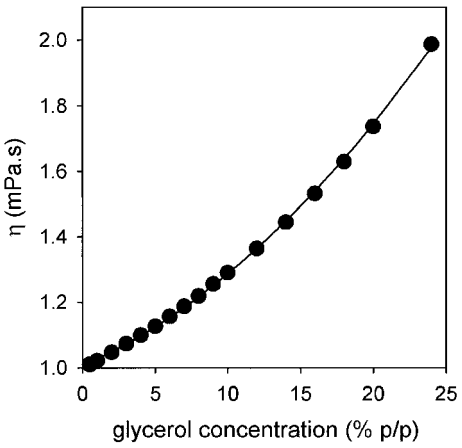

FIG. 1. **Viscosity of aqueous solutions of glycerol.** The viscosity coefficient at 20 °C of glycerol-water solutions are plotted as a function of the glycerol concentration (*c*). A second-degree polynomial was fitted to these data, obtaining the following equation: $\eta = 0.000867\ c^2 + 0.0191\ c + 1.007$. The *continuous line* is the graphical representation of this equation.

the obtained function. Samples were equilibrated at 20 °C for 20 min before measuring the anisotropy.

Spectroscopic Measurements—Fluorescence measurements were performed at 20 °C using a SLM-Aminco Bowman Series 2 (SLM, Urbana, IL) spectrofluorometer equipped with excitation and emission polarizers.

Fluorescence anisotropy was measured, setting the excitation at 340 nm and the emission at 470 nm, with bandwidths of 4 nm. Anisotropy was calculated using Equation 1, including the instrument *G* factor defined as the ratio of sensitivities of the detection system for the vertically and horizontally polarized light [3],

$$r = \frac{I_{VV} - G \cdot I_{VH}}{I_{VV} + 2 \cdot G \cdot I_{VH}}, \text{ with } G = \frac{I_{HV}}{I_{HH}} \qquad \text{(Eq. 5)}$$

where *H* and *V* refer to the horizontal and vertical positions, respectively, of the excitation (first subscript) and emission (second subscript) polarizers.

Data Analysis—Equations were fitted to the experimental data using a nonlinear regression procedure [10]. The dependent variable was assumed to be homoscedastic (constant variance), and the independent variable was considered to have negligible error. Parameters were expressed as the mean ± S.E.

Structure of Class Activities—The laboratory class was organized into three blocks of approximately 90 min each. In the first block, the students (in small groups) discussed the experimental design and prepared the samples to be measured. In the second block, they registered the data. A final discussion was then held in the groups and extended to the whole class.

RESULTS AND DISCUSSION

Measurement of Dansyl Anisotropy—In a previous laboratory class [9], students analyzed the absorption and emission spectra of dansyl-BSA. Based on these data, they chose adequate excitation and emission wavelengths to measure the fluorescence anisotropy of dansyl attached to BSA. After this, they registered the fluorescence intensity of 30 μM dansyl-BSA or dansyl-Tris solutions at the selected wavelengths, after sequential changes of the polarizers positions to horizontal and vertical. The calculated fluorescence anisotropies were 0.219 ± 0.002 (dansyl-BSA) and 0.001 ± 0.003 (dansyl-Tris).

It can be observed that the anisotropy of dansyl-Tris is not significantly different from zero, indicating that the probe reached a random distribution within its lifetime when it is bound to the small Tris molecule. Conversely, the anisotropy of dansyl bound to BSA is significantly higher, suggesting that the mobility of the probe is restricted by attachment to the macromolecule.

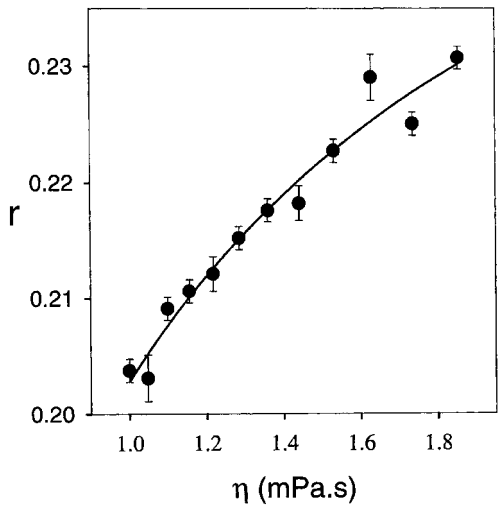

FIG. 2. **Dependence of dansyl-BSA anisotropy on the viscosity of the solution.** Dansyl-BSA anisotropy is represented as a function of the viscosity of the solutions (for experimental details, see *Materials and Methods*). The *continuous line* is the graphical representation of Equation 4 with the best fitting parameter values indicated in the text.

TABLE II
Molecular size and hydration degree of some macromolecules

	M_r	V (nm^3)	R_S (nm)	δ_{max}	δ_{exp}	V_h (nm^3)
BSA	66,430	163	3.4	0.74	0.40	125
Lysozyme	14,100	37	2.1	0.88	0.34	24
Ovalbumin	45,000	88	2.8	0.43	0.33	81
Hemoglobin	68,000	125	3.1	0.36	0.42	132
Chymotrypsinogen	23,200	48	2.2	0.52	0.33	41
DNA	6,000,000	$1.9 \cdot 10^7$	165	1890	0.59	$1.12 \cdot 10^4$

Dependence of Dansyl-BSA Anisotropy on the Viscosity—Figure 2 shows the dansyl-BSA anisotropy values measured after changing the viscosity of the solution by the addition of glycerol. As expected, *r* increased with increasing the viscosity. By fitting Equation 4 to the experimental data, students obtained the following parameter values: $r_o = 0.273 \pm 0.004$ and $c = 0.347 \pm 0.027$ mPa·s.

The limiting anisotropy r_o correspond to the hypothetical situation in which the viscosity of the medium is infinitum, that is, in the absence of rotational motions. Although the r_o value is obtained by extrapolation of the experimental data, its high value suggests a small angle between the absorption and emission moments.

Considering that the lifetime of dansyl attached to BSA is 14 ns [11], students calculated the rotational correlational time of BSA in the absence of glycerol, obtaining $\phi = 40 \pm 3$ ns. This means that, after 40 ns of excitation, dansyl-BSA molecules rotated, on average, 68 degrees with respect to the initial orientation. As a consequence, the fluorescence anisotropy decreased up to $r_o \cdot e^{-1}$ [5].

On the other hand, the volume of the hydrodynamically equivalent sphere can be calculated from the parameter *c*

$$V = \frac{\tau \cdot k \cdot T}{c} = 163 \pm 13 \text{ nm}^3 \qquad \text{(Eq. 6)}$$

From this value, a Stokes radius (R_s) of 3.39 ± 0.27 nm is derived for the BSA molecule. This value is consistant with the value determined by other techniques as traslational diffusion (3.52 nm) [12, 13] and gel filtration (3.48 nm) [14].

Further Discussion— According to a classic hydrodynamic analysis [2, 12, 15], the hydrated volume of a molecule is given by

$$V_h = \frac{Mr}{N} \cdot (v_2 + \delta \cdot v_1^0) \qquad \text{(Eq. 7)}$$

where v_2 is the partial specific volume of the macromolecule, v_1^o is the specific volume of water, and δ is the degree of hydration.

Supposing that the volume calculated according to Equation 6 corresponds to the hydrated volume of BSA (which implies it approximates the BSA shape to a sphere), we can determine the maximum degree of protein hydration from Equation 7. Taking into account that Mr_{BSA} = 66,430; v_1^o = 1.0018 cm^3/g; and v_2 = 0.734 cm^3/g [12]; students solved Equation 7 obtaining δ_{max} = 0.74. This value is consistant with values estimated from measurements of intrinsic viscosity (δ_{max} = 0.75) and translational diffusion (δ_{max} = 1.07) [12]. However, these values are significantly higher than δ_{exp} = 0.4, the degree of hydration experimentally determined by NMR [13].

Equation 7 can also be used to calculate the volume of the hydrated BSA molecule (V_h) from the values of M_r, v_2, δ_{exp}, and v_1^o. This procedure does not assume any specific shape for the BSA molecule. Students performed this calculation, obtaining a value of 125 nm^3. The difference between this value and that previously calculated for the hydrodynamically equivalent sphere (V) can be explained in terms of either a slight molecular asymmetry of BSA [12] or the involvement of dimer monomer equilibrium [16].

Table II summarizes the data of V, R_s and δ_{max} for BSA determined by the students and data corresponding to other macromolecules under the spherical approximation [2, 12]. Table II also includes the experimental degree of hydration (δ_{exp}) of these proteins and the hydrated volumes (V_h) calculated by following a procedure similar to that described above for BSA.

It can be observed that, for globular proteins, the spherical approximation gives volume values close to the hydrated volumes, but, for very asymmetric molecules such as DNA, the difference between both volumes is very large.

CONCLUDING REMARKS

This laboratory class has been successfully implemented during 3 years in undergraduate courses of biophysical chemistry. Students found that the simplicity of the experiment and data analysis allowed them to focus in the relationship between probe anisotropy and rotational diffusion. An excellent review on the principles and applications of fluorescence polarization [17] has been recently published. The authors recommend this review as a complement to the discussion proposed in this article.

REFERENCES

[1] R. P. Feynman, R. B. Leighton, M. L. Sands (1963) The Feymann Lectures on Physics, Mainly Mechanics, Radiation and Heat, Addison-Wesley, Reading, Massachusetts, pp. 33.1–33.10.
[2] C. R. Cantor, P. R. Schimmel (1980) Biophysical Chemistry, W. H. Freeman, New York, pp. 125–167.
[3] B. Valeur (2001) Molecular Fluorescence: Principles and Applications, Wiley, New York, pp. 125–167.
[4] G. Weber (1953) Rotational Brownian motion and polarization of the fluorescence of solutions, *Adv. Protein Chem.* **8**, 415–459.
[5] K. E. Van Holde, W. C. Johnson, P. S. Ho (1998) Principles of Physical Biochemistry, Prentice Hall, New Jersey, pp. 452–483.
[6] G. Weber (1952) Polarization of the fluorescence of macromolecules. I. Theory and experimental method, *Biochem. J.* **51**, 145–155.
[7] S. Baud, E. Margeat, S. Lumbroso, F. Paris, C. Sultan, C. Royer, N. Poujol (2002) Equilibrium binding assays reveal the elevated stoichiometry and salt dependence of the interaction between full-length human sex-determining region on the Y chromosome (SRY) and DNA, *J. Biol. Chem.* **277**, 18404–18410.
[8] M. F. Engel, C. P. van Mierlo, A. J. Visser (2002) Kinetic and structural characterization of adsorption-induced unfolding of bovine alpha-lactalbumin, *J. Biol. Chem.* **277**, 10922–10930.
[9] V. Levi, F. L. Gonzalez Flecha (2003) Labeling of proteins with fluorescent probes. Photophysical characterization of dansylated bovine serum albumin. *Biochem. Mol. Biol. Educ.* **31**, 333–336.
[10] G. A. F. Seber, C. J. Wild (1989) Nonlinear Regression, John Wiley & Sons, New York, pp. 21–27.
[11] G. Weber (1952) Polarization of the fluorescence of macromolecules. II. Fluorescent conjugates of ovalbumin and bovine serum albumin, *Biochem. J.* **51**, 155–167.
[12] C. Tanford (1961) Physical Chemistry of Macromolecules, Wiley, New York, pp. 317–456.
[13] I. D. Kuntz, W. Kauzmann (1974) Hydration of proteins and polypeptides, *Adv. Protein Chem.* **28**, 239–345.
[14] I. Axelsson (1978) Characterization of proteins and other macromolecules by agarose gel chromatography *J. Chromatogr. A* **152**, 21–32.
[15] I. Tinoco, K. Sauer, J. C. Wang, J. D. Puglisi (2002) Physical Chemistry: Principles and applications in biological sciences, Prentice Hall, New Jersey.
[16] V. Levi, F. L. González Flecha (2002) Reversible fast-dimerization of bovine serum albumin detected by fluorescence resonance energy transfer, *Biochim. Biophys. Acta.* **1599**, 141–148.
[17] D. M. Jameson, J. C. Croney (2003) Fluorescence polarization: past, present, and future, *Comb·Chem·High Throughput Screen* **6**, 167–173.